Journal of *Marine Science and Engineering*

MDPI

Article

Sedimentological and Petrographical Characterization of the Cambrian Abbottabad Formation in Kamsar Section, Muzaffarabad Area: Implications for Proto-Tethys Ocean Evolution

Syed Kamran Ali [1,*], Rafiq Ahmad Lashari [2], Ali Ghulam Sahito [2], George Kontakiotis [3,*], Hammad Tariq Janjuhah [4], Muhammad Saleem Mughal [1], Ahmer Bilal [5], Tariq Mehmood [6] and Khawaja Umair Majeed [1]

1 Institute of Geology, Azad Jammu and Kashmir University, Muzaffarabad 13100, Pakistan
2 Center for Pure and Applied Geology, University of Sindh, Jamshoro 76060, Pakistan
3 Department of Historical Geology and Paleontology, Faculty of Geology and Geoenvironment, National and Kapodistrian University of Athens, Panepistimiopolis, 15784 Athens, Greece
4 Department of Geology, Shaheed Benazir Bhutto University, Sheringal 18050, Pakistan
5 Shandong Provincial Key Laboratory of Depositional Mineralization & Sedimentary Minerals, Shandong University of Science and Technology, Qingdao 266590, China
6 Oil and Gas Development Corporation Limited (OGDCL), Islamabad 44000, Pakistan
* Correspondence: kamran.ali@ajku.edu.pk (S.K.A); gkontak@geol.uoa.gr (G.K.)

Abstract: The current sedimentological and petrographical research of the Abbottabad Formation has been carried out in order to understand the formation and evolution of the Proto-Tethys Ocean during the Cambrian on the northern margin of the Indian Plate. The Muzaffarabad region is located east of the Upper Indus Basin and the southern part of the Hazara Kashmir Syntaxis. The geological history of the region varies from the Precambrian to the recent period. The Cambrian Abbottabad Formation is well exposed along the Hazara Kashmir Syntaxis at the core of the 500-m-thick Muzaffarabad anticline. The Abbottabad Formation is an unconformity-bounded allo-stratigraphic unit. It has an unconformable lower contact with the Late Precambrian Dogra Formation and an unconformable upper contact with the Paleocene Hangu Formation. The Abbottabad Formation has been divided into four lithofacies, from bottom to top, namely, thinly interbedded dolomite and shale, cherty-stromatolitic dolomite, oxidized limonitic-brecciated zone, and quartzite, with significant lithological changes. Petrographic studies revealed four types of dolomites: fine crystalline dolomite (Dol. I), dolomitic cryptocrystalline chert (Dol. II), algal mat-stromatolitic dolomite (Dol. III), and intraclastic-dolo-grain stone (Dol. IV). The mineral composition of dolostone was analyzed using X-ray diffraction (XRD) and found to be consistent with previous petrographic studies. The dolomite mineral content decreased from base to top, while chert increased towards the top. Elemental weight percentages through energy dispersive X-ray (EDX) analysis show different elements constitute the minerals found in the dolostone, as confirmed by petrographic and XRD analysis. Using outcrop data, facies information, and geochemical data, a modified depositional model of the Abbottabad Formation was developed. During the Early Cambrian period, the formation was deposited in a shallow subtidal to supratidal setting of the Proto-Tethys Ocean. The top of this deposit marks the Cambrian–Paleocene boundary. Because of the progressively coarsening outcrop sequences, this formation seems to be at the very top of the Proto-Tethys Ocean's shallow marine system.

Keywords: stromatolites; dolomite microfacies; Proto-Tethys Ocean; shallow marine carbonates; subtidal-supratidal depositional environments; sequence stratigraphic development; sedimentary basin dynamics; stratigraphic correlations; diagenetic processes; paleoenvironmental reconstruction

Citation: Ali, S.K.; Lashari, R.A.; Sahito, A.G.; Kontakiotis, G.; Janjuhah, H.T.; Mughal, M.S.; Bilal, A.; Mehmood, T.; Majeed, K.U. Sedimentological and Petrographical Characterization of the Cambrian Abbottabad Formation in Kamsar Section, Muzaffarabad Area: Implications for Proto-Tethys Ocean Evolution. *J. Mar. Sci. Eng.* **2023**, *11*, 526. https://doi.org/10.3390/jmse11030526

Academic Editor: Dimitris Sakellariou

Received: 7 January 2023
Revised: 23 February 2023
Accepted: 27 February 2023
Published: 28 February 2023

1. Introduction

The Himalayas are classified into four subdivisions, i.e., sub-Himalaya, lesser Himalaya, higher Himalaya, and trans-Himalaya [1]. The Muzaffarabad area situated in the east of the Upper Indus Basin (UIB) in Pakistan [2] and is the southern portion of the Hazara Kashmir Syntaxis (HKS), sub-Himalaya (Figure 1). The HKS of the Northern Pakistan has been the focus of geological study because of its sedimentology, complicated structure, and seismicity. The area is highly deformed by the folds and faults owing to tectonic activity [3]. The sedimentological sequence ranges in age from Cambrian to the most recent era. The inner core of the HKS mainly consists of the Cambrian Abbottabad Formation, which is thrust over the Miocene Murree Formation [3]. The study area forms the core and the northern limb of a Muzaffarabad overturned anticline, which is part of regional HKS in the Muzaffarabad city along Neelum valley road, Azad Jammu and Kashmir, Pakistan (AJKP).

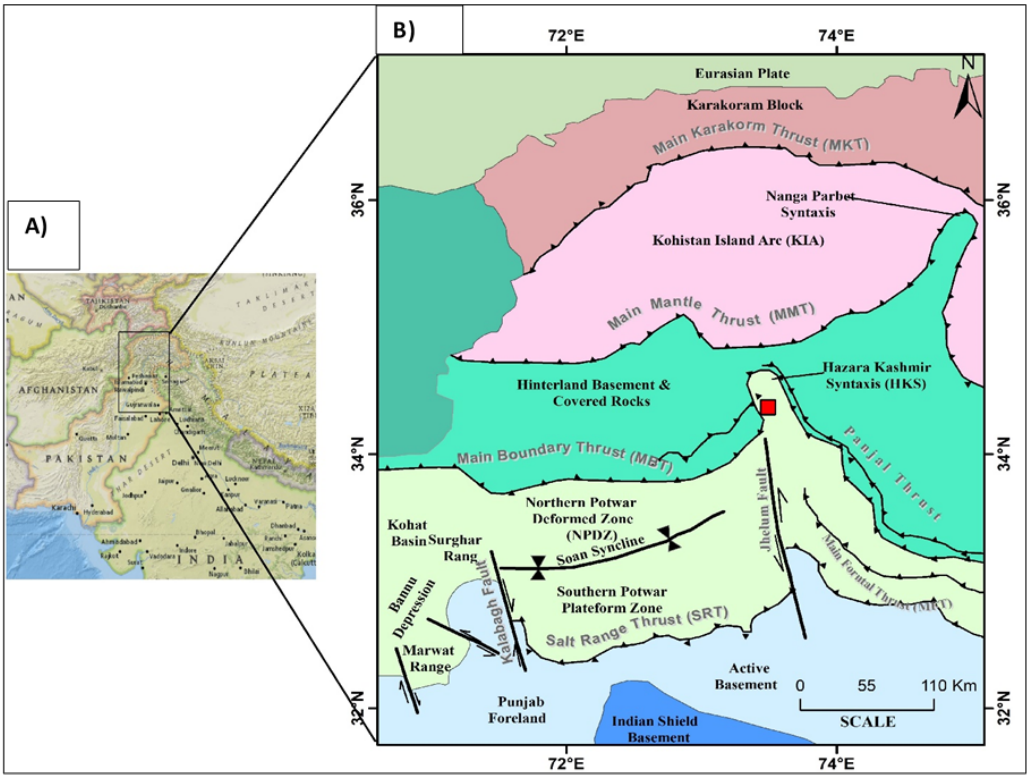

Figure 1. (**A**) Regional location map of the northern Pakistan; (**B**) tectonic map of northern Pakistan. Red square showing the study area (compiled and adopted after [4–6]).

Various researchers have worked on the stratigraphy and tectonics of HKS deposits in different parts of Azad Jammu and Kashmir, Pakistan (AJKP) [3–5,7–18]. The geology and stratigraphy of this region was originally described by Medlicott [19]. The Swiss geologist Bossart, et al. [20]) described the lithological, stratigraphic and structural features of HKS. Greco [8] described the stratigraphic and metamorphic features of the rocks of the Hazara-Kashmir Syntaxis. Baig and lqbal Siddiqi [9] and Baig, et al. [21] worked on the Muzaffarabad fault and discussed the active tectonic evidence.

Although general information about the stratigraphic and sedimentological aspects of the various formations in the HKS exists, detailed study regarding sedimentology and stratigraphy for the dolomites of the Abbottabad Formation is lacking, which is crucial for understanding the Cambrian deposits of Proto-Tethys Ocean in the northern Pakistan. The Abbottabad Formation was selected for sedimentological and petrographic analysis. The Abbottabad Formation consists of stromatolitic, thinly to thickly bedded dolomite of the Cambrian age. Different researchers presented various models for the genesis of dolomite and the associated diagenetic environment [22–27].

This study aims to determine the litho- and micro-facies of dolostone, its depositional environment, and stromatolite development in the Abbottabad Formation. The depositional model proposed here will provide additional insights into the paleogeographic evolution of the Proto-Tethys basin and a better correlation with nearby tectonostratigraphic successions.

2. Geological Framework

The study area lies in the Kamsar to Yadgar region of the Muzaffarabad, a division of AJKP and is part of HKS (Figure 1). The HKS is one of the most conspicuous northwest Himalayan structures and is a complex tectonic zone formed by a regional shift in the northeast-to-northwest strike of orogeny. The syntaxial zone and its surroundings exhibit sedimentary, volcanic, and metamorphic rocks from the Precambrian to the Neogene [5]. The thickness of the Precambrian and Cambrian rock strata increases eastward from the UIB while it diminishes westward (Figure 2) [28]. The HKS comprises numerous thrust sheets that overlap and are composed of Precambrian to Mesozoic formations that were thrust onto molasses deposits [13,29,30].

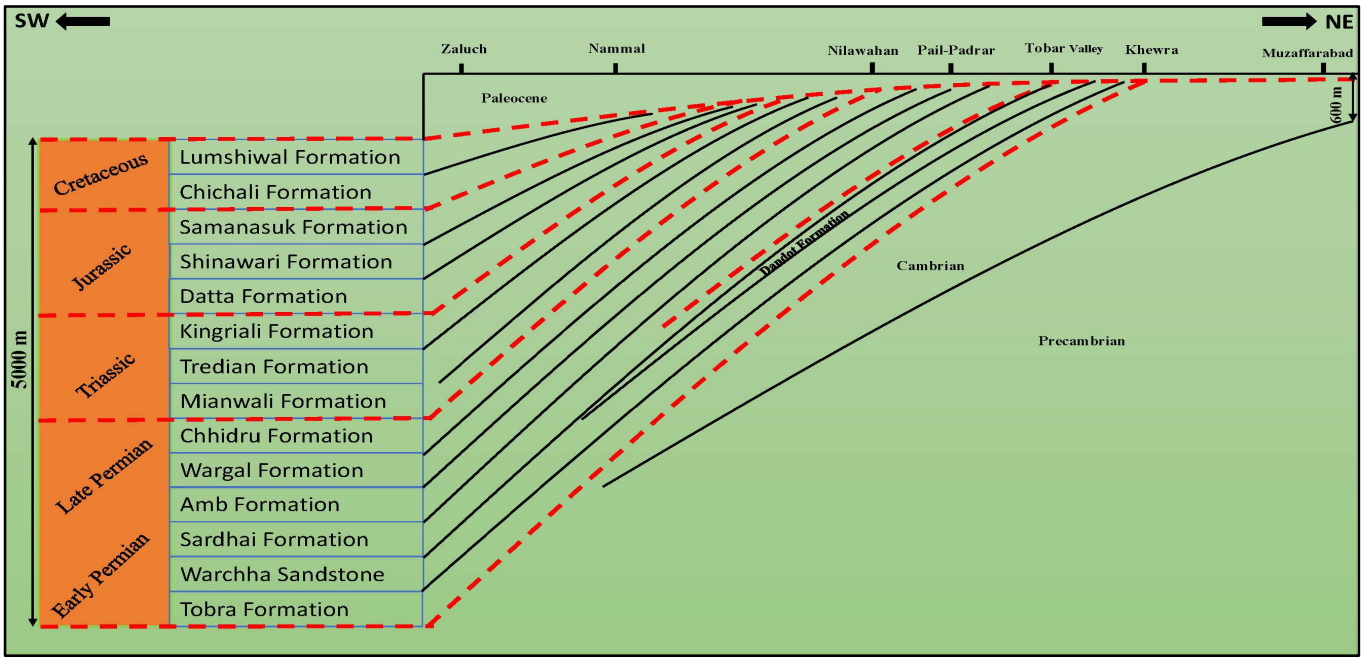

Figure 2. Surface and subsurface deposition of different formations and unconformities in UIB and HKS.

In the Cambrian period, the study region was a part of Gondwanaland characterized by generally warm, shallow marine environments [29,30]. After a period of non-deposition during the Lower Cambrian, the region once again experienced a transgression of the sea and the deposition of the Abbottabad Formation took place [28]. The Ordovician to Cretaceous rock sequence was not deposited during tectonic uplift and erosion related to earlier orogenic events on the Gondwana of the Indian Plate (Figure 2) [31]. In the early Paleocene, the Hangu Formation was deposited at the base of the Late Paleocene–Early Eocene Neo-Tethys limestone and shale sequence [32]. After the collision of the Indo-Eurasian plates in the Cretaceous, the regional thrust systems evolved, including the Main Karakoram Thrust (MKT), the Main Mantle Thrust (MMT), the Main Boundary Thrust (MBT), and the Salt Range Thrust (SRT) [1,33,34]. Currently, the research area is in the sub-Himalayas. The Main Boundary Thrust (MBT) restrains the sub-Himalayan lithosphere from the north. The MBT divides the rocky regions of the sub-Himalayan area from the lesser Himalayan region (Figure 1).

Stratigraphy of Kamsar Section Abbottabad Formation

The study area contains rocks from the Precambrian Dogra Formation to the Miocene Murree Formation (Figure 3). The majority of the Dogra Formation is composed of graphitic schist, phyllite, and marble. The uppermost contact between the Dogra Formation and the Abbottabad Formation is nonconformable, and the Abbottabad Formation marks the beginning of the Cambrian period.

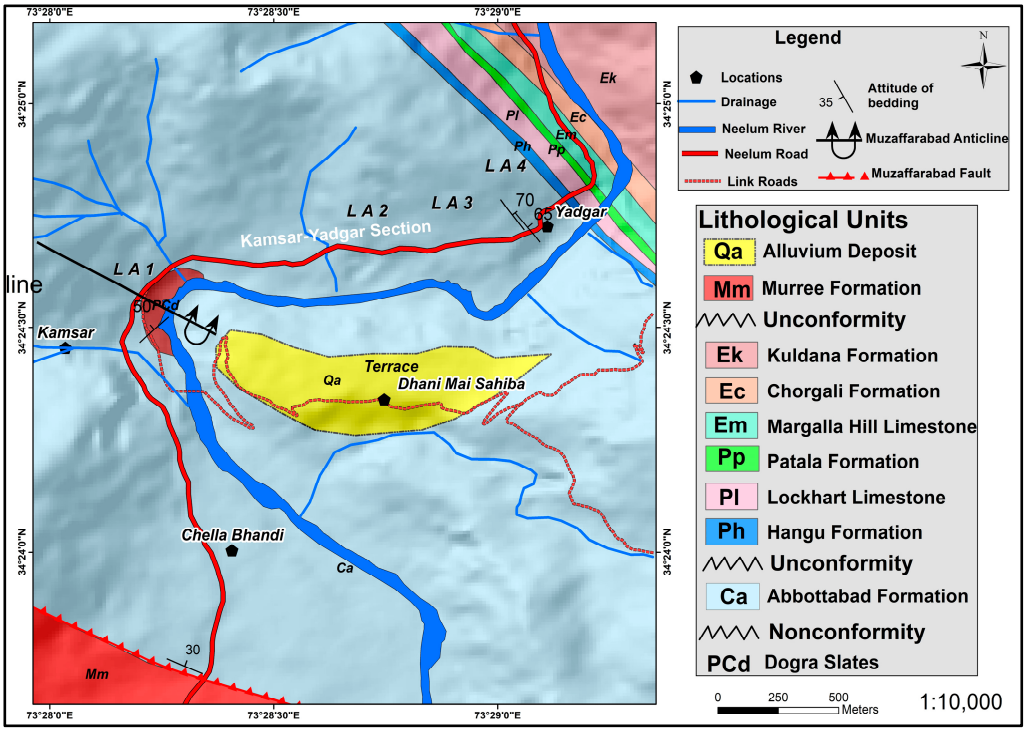

Figure 3. Simplified geological map of the study area.

The Stratigraphic Committee of Pakistan has classified the primarily dolomite, quartzite, and limestone rocks of the Abbottabad district as the Abbottabad Formation [35]. This nomenclature has been expanded to encompass the similar and correlative rocks previously referred to as "great limestone" [36], "Upper Dolomite Member" [7], "Muzaffarabad Formation" [4], and the Sirban Formation [8]. In the study area, the Abbottabad Formation is exposed under the MBT in the sub-Himalaya region and the center of the Muzaffarabad anticlinal system. This formation consists of cliffs and very steep slopes and have average thickness of 200–833 m [37].

The Abbottabad Formation is composed mostly of cherty dolomite, with subordinate shales, stromatolitic dolomite, and quartzite facies. Latif [14] identified a few Cambrian-aged fossils in the Abbottabad Formation, which is mostly fossil-free. The microfossils in the Abbottabad Formation are interpreted to reflect the Cambrian Period. About 500 mya, after the Cambrian deposit ended, the Paleocene deposit began. Overlying the Abbottabad Formation, the Hangu Formation's bauxite, coal seams, and sandstone deposits with average thickness of 15–35 m [37] indicate the primary unconformity at the erosional breccia surface of dolomite [13].

3. Methodology

3.1. Field Study

Field observations were conducted in Muzaffarabad's Kamsar-Yadgar region (Figure 3). This investigation shows a variety of outcrop lithofacies. Using Jacob's staff technique, the outcrops of the Abbottabad Formation were recorded, sampled, and measured. Based on sedimentological observations, such as lithological variations, color, and depositional

texture, detailed investigations were performed to identify distinct lithofacies (Table 1). A total of 100 samples from the Abbottabad Formation were obtained from different places.

Table 1. Litho facies of the Abbottabad Formation, Kamsar-Yadgar section, Muzaffarabad.

Lithofacies	Description	Bedding and Structures	Environment of Deposition
LA-1 Dolomite with subordinate shale	The basal zone is fine grained, light grey dolomite. The upper zone consists of dark grey, thinly bedded dolomite with blackish shales.	Lenticular layers with minor erosional surfaces against shale; small-scale cross-lamination; rare normal graded bedding.	Shallow subtidal
LA-2 Stromatolitic dolomite member	This zone is typical dolomite showing growth of thinly laminated algal mats to thick domal shape stromatolites. The colour of the dolomite is light grey with some chert bands.	Convex to undulatory laminae; abundant stromatolites of varying shapes and size; large domal and columnar stromatolites up to 10 to 15 cm, 1–2 m long and grading upwards into microbial laminae.	Shallow subtidal to supratidal
LA-3 Oxidized, ferruginous, dolomite	This zone is greenish and reddish brown, rusty stained, brecciated, and limonitic. The thickness of this zone at Yadgar is 16.2 m and extends more than 100 m along dip and strike.	Monomict with lithology, such as host rocks as well as dolomite and chert clasts; poorly sorted, sub-angular to angular clasts of varying sizes and coated by oxidized limonite.	Surface karstification products; karstic depression fills
LA-4 Quartzite member	Quartzite is fine grained, snow white to white, with brownish to yellowish encrustations on the joints.	The thickness of the quartzite varies from 9 to 25 m and brecciated at the top. Calcrete deposits.	Subaerial exposure

3.2. Petrography

Thin sections of dolomitic rock were prepared at the Hydrocarbon Development Institute of Pakistan (HDIP) in Islamabad. A petrographic microscope (Leica DM-750P) was used to examine thin sections for mineral identification and diagenetic markers using reflected and transmitted light. Tables 2 and 3 show the results of the modal mineralogical composition using the point-counting technique. Photomicrographs were taken and used to characterize microfacies. The basic terminology of dolomite textures employed in thin sections considers crystal structure, crystal mutual relationships, and uniform or non-uniform size distribution. Commonly, dolomite has an idiotopic (planar) to a xenotopic (non-planar) texture. The idiotopic texture is further divided into idiotopic e, idiotopic s, idiotopic c, and idiotopic p, representing euhedral, subhedral, cement, and porphyrotopic, respectively. The xenotopic texture is further classified into xenotopic a, xenotopic c, and xenotopic p, indicating anhedral, cement with saddle shaped dolomite crystals, and porphyrotopic, respectively. Saddle dolomite derived from hydrothermal fluids is a late diagenetic product that often overprints earlier diagenetic phases. The carbonate classification methods of Dunham [33], Sibley and Gregg [34] and Flügel and Munnecke [37] were used to analyze the texture and microfacies of the carbonate rocks, which comprised both biogenic and inorganic dominant components. The classification technique of Logan, et al. [38] was used to classify stromatolites. Kalkowsky [39] used the term stromatolith to describe "limestone masses with a thin, planar layered structure", composed of a collection of laminae ("stromatoid") thought to be of vegetal origin. Logan, Rezak and Ginsburg [38] developed a classification to characterize the growth types of intertidal and shallow subtidal stromatolites. Laminated mats are frequent in quiet-water supratidal and intertidal environments, whereas domal growth forms are widespread in subtidal conditions. Several petrographic observations and diagenetic phases were documented and quantified to analyze the depositional environment using lithofacies analysis. Figure 4 presents a summary of the results based on the above sedimentological and petrographic observations.

Table 2. Modal mineralogical composition of the Abbottabad Formation, Kamsar section, Muzaffarabad.

Sr. No.	Sample No.	Dol	Chert	Cr. Silica	Chl	Calcite	Pr	CM	St	Hm	BC	Sc	IC	Mc	Pl	Microfacies
1	KA-1	70	–	–	–	–	–	30	–	–	–	–	–	–	–	Dol. I
2	KA-2	90	5	–	–	–	5	–	–	–	–	–	–	–	–	Dol. I
3	KA-3	75	5	–	1	–	4	–	15	–	–	–	–	–	–	Dol. I
4	KA-4	90	1	–	–	4	–	–	–	3	2	–	–	–	–	Dol. I
5	KA-5	30	5	40	20	3	2	–	–	–	–	–	–	–	–	Dol. II
6	KA-8	75	5	–	–	–	5	15	–	–	–	–	–	–	–	Dol. III
7	KA-19	90	1	–	–	9	–	–	–	–	–	–	–	–	–	Dol. I
8	KA-22	85	5	–	–	–	2	8	–	–	–	–	–	–	–	Dol. I
9	KA-27	75	20	–	4	–	1	–	–	–	–	–	–	–	–	Dol. I
10	KA-31	95	1	–	–	–	–	–	–	2	1	1	–	–	–	Dol. I
11	KA-35	78	10	–	–	–	2	10	–	–	–	–	–	–	–	Dol. III
12	KA-37	65	15	–	2	15	–	–	–	3	–	–	–	–	–	Dol. I
13	KA-41	–	25	65	8	–	–	–	–	2	–	–	–	–	–	Dol. II
14	KA-44	70	5	–	3	20	–	–	–	2	–	–	–	–	–	Dol. I
15	KA-50	20	5	–	–	–	1	–	–	–	–	–	60	12	2	Dol. IV

Abbreviations: Dol = dolomite, Cr. Silica = cryptocrystalline silica, Chl = chalcedony, Pr = pyrite, CM = carbonaceous material, St = stylolite features, Hm = hematite, BC = bioclast, Sc = sericite, IC = intraclasts, Mc = micrite, Pl = peloids.

Table 3. Modal mineralogical composition of the Abbottabad Formation, Kamsar section, Muzaffarabad.

Sr. No	S. No.	Dol	Chert	Cr. Sil.	Chl	CM	Calcite	Pr	Pl	IC	Qtz	Sp	Mc	Hm	BC	Oo	Zr	Tr	Apt	Opm	Microfacies
1	KA-56	30	20	–	5	5	–	–	–	10	–	15	15	5	–	–	–	–	–	–	Dol. III
2	KA-59	–	20	60	–	–	–	15	–	–	–	–	–	–	–	–	–	–	–	–	Dol. II
3	KA-60	30	60	–	–	–	–		–	–	–	–	–	5	5	–	–	–	–	–	Dol. II
4	KA-61	5	50	30	5	–	–	10	–	–	–	–	–	–	–	–	–	–	–	–	Dol. II
5	KA-63	18	30	–	5	7	–	5	25	–	–	–	–	2	–	5	1	1	1	–	Dol. III
6	KA-65	25	–	–	10	–	–	–	–	25	25	13	–	–	–	–	–	1	–	1	Dol. IV
7	KA-66	65	–	–	5	20	5	2	–	–	–	–	–	3	–	–	–	–	–	–	Dol. III
8	KA-67	50	4	–	5	15	7	–	15	–	–	–	–	3	1	–	–	–	–	–	Dol. III
9	KA-68	–	20	60	10	–	–	–	–	–	–	–	–	10	–	–	–	–	–	–	Dol. II
10	KA-69	73	–	–	5	7	10	–	–	–	–	–	–	5	–	–	–	–	–	–	Dol. III
11	KA-70	75	5	–	–	5	–	7	–	–	–	–	–	3	5	–	–	–	–	–	Dol. III
12	KA-76	20	20	–	–	–	–	–	–	5	55	–	–	–	–	–	–	–	–	–	Dol. IV
13	KA-82	–	3	–	–	–	–	–	–	–	95	–	–	–	–	–	–	1	–	1	Arenite
14	KA-84	15	15	45	24	–	–	–	–	–	–	–	–	1	–	–	–	–	–	–	Dol. II
15	KA-87	3	–	–	–	–	–	–	–	–	95	–	–	–	–	–	–	1	–	1	Arenite

Abbreviations: Dol = dolomite, Cr. Sil. = cryptocrystalline silica, Chl = chalcedony, CM = carbonaceous material, Pr = pyrite, Pl. = peloids, IC = intraclasts, Qtz. = quartz, Sp = spar, Mc = micrite, Hm = hematite, BC = bioclast, Oo = ooid, Zr = zircon, Tr = tourmaline, Apt = apatite, Opm = opaque minerals.

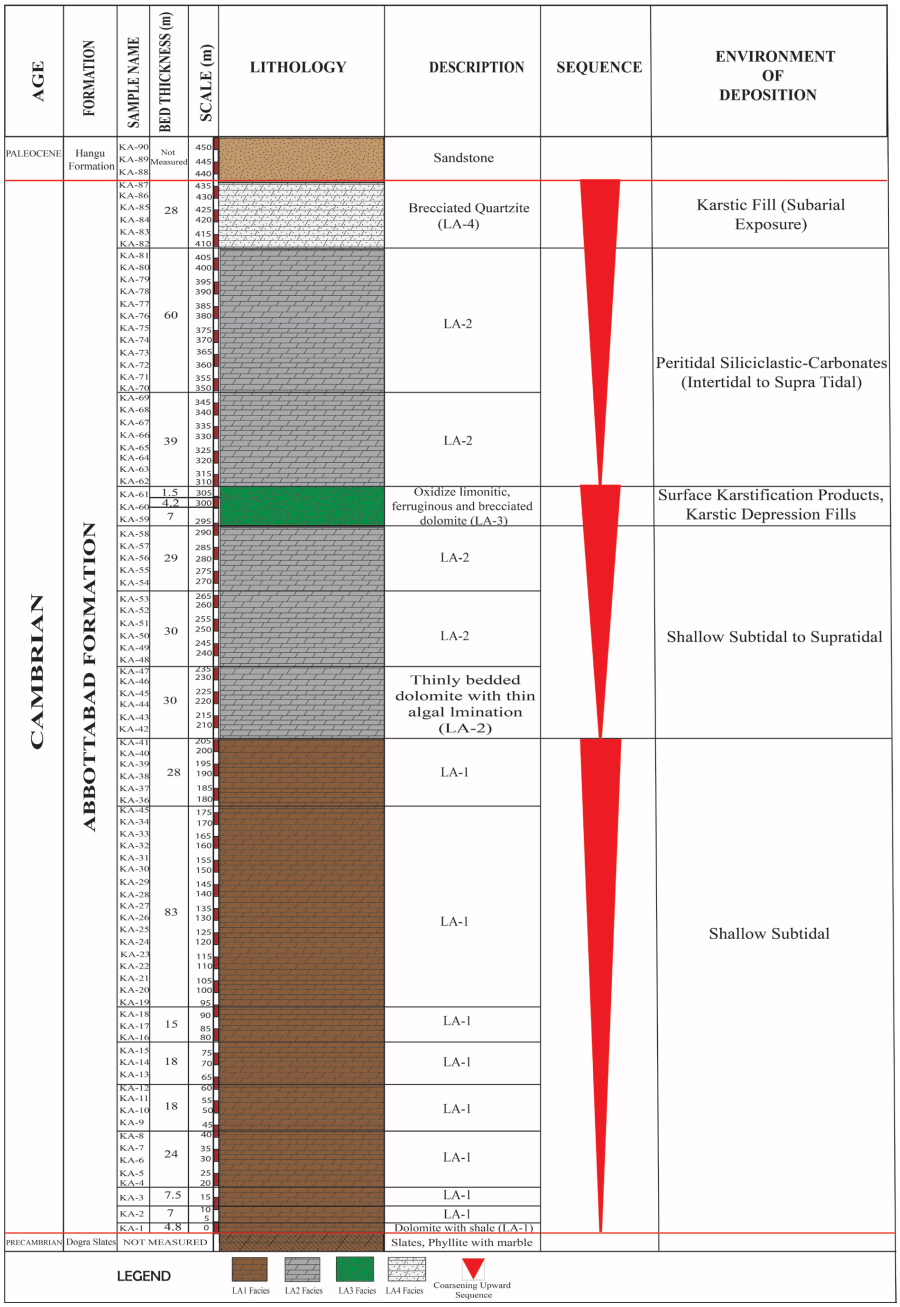

Figure 4. Litho-log of the Kamsar-Yadgar section, Muzaffarabad, Pakistan.

3.3. X-ray Diffraction (XRD) Energy Dispersive X-ray (EDX)

For the current research work, four samples of dolomite from the Abbottabad Formation were taken for XRD and eight samples for EDX analysis. The samples for XRD analysis were sent to Centralized Resource Laboratory (CRL), Peshawar University, and samples for EDX analysis were sent to Laboratory of Center for Pure and Applied Geology, University of Sindh, Pakistan, where they underwent detailed analysis.

The X-ray diffraction (XRD) instrument utilized at CRL Peshawar was a JDX-3532 Diffractometer from Japan with the capacity to generate voltages ranging from 20 to 40 kV and currents ranging from 2.5 to 30 mA. The instrument employed a copper (CuKa) X-ray source with a wavelength of 1.5418 nm and a 2Theta-range of 0–160°. Copper is a widely used X-ray source, and its K peak at 1.5418 nm offers advantages for analyzing minerals due to its higher-order lattice spacing, which is 10–15 times greater than the wavelength. Finally, the XRD data were analyze by Jade 6.5 software.

To perform EDX analyses, the samples were first coated with gold using the DII-29030SCTR smart coater, and then analyzed using a JEOL EDS system with Bruker software.

4. Results

4.1. Litho- and Petro-Facies Characterization of the Abbottabad Formation

The Abbottabad Formation has a non-conformable lower contact with the Precambrian Dogra slates in the study area (Figures 4 and 5A), while the Palaeocene Hangu Formation unconformably overlies the Abbottabad Formation (Figure 5I).

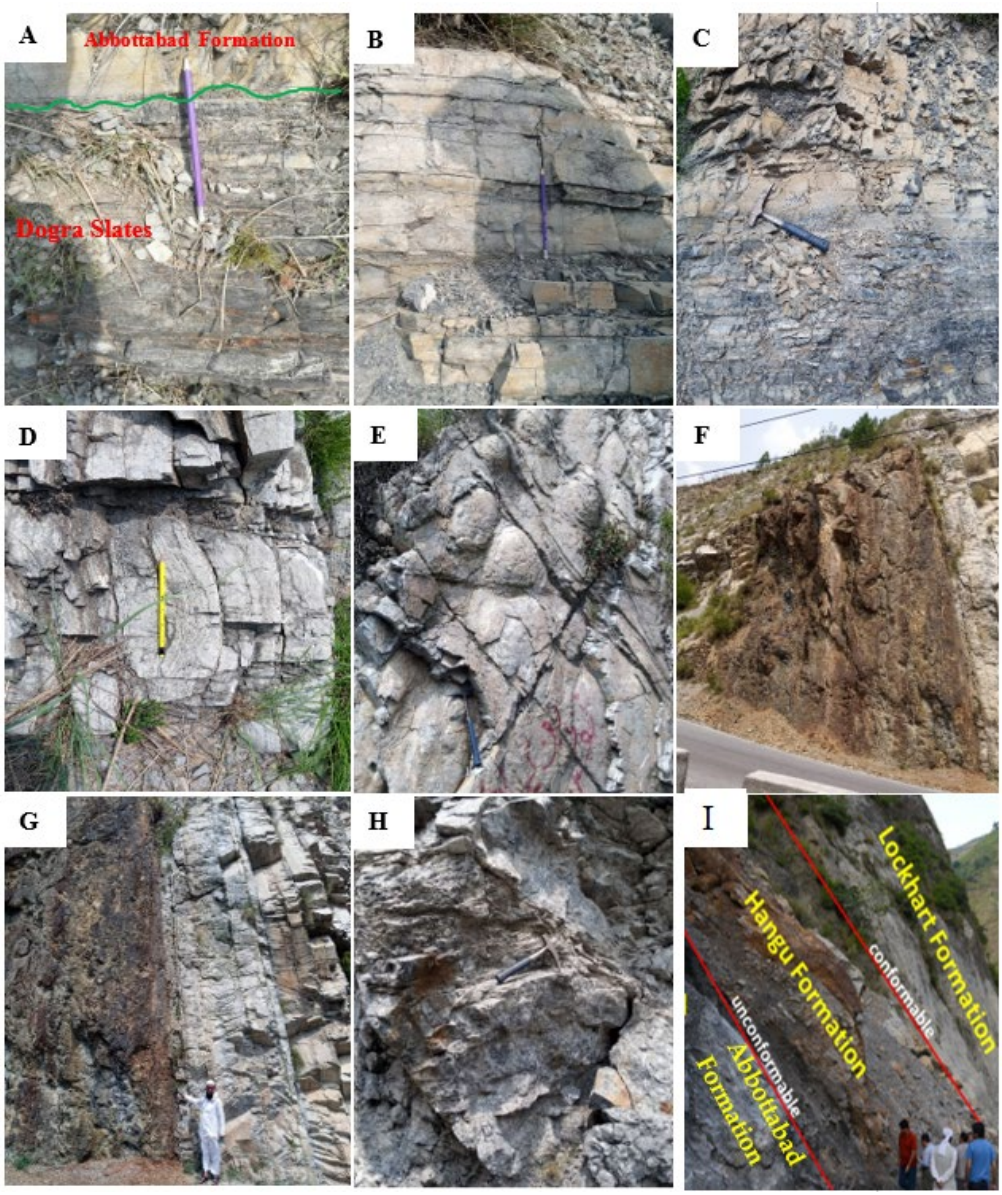

Figure 5. Detailed field characteristics and lithofacies of the Abbottabad Formation at Kamsar-Yadgar section, Muzaffarabad: (**A**) non-conformable contact between the Dogra slate and thin interbedded dolomite of the Abbottabad Formation (LA-1); (**B**) thinly bedded dolomite with blackish shale (LA-1); (**C**) thinly bedded greyish dolomite (LA-1); (**D**) thinly laminated convex algal mats (LA-2); (**E**) thick dome-shaped stromatolites (LA-2); (**F**) reddish brown, rusty stained, brecciated, and highly limonitic dolomitic zone (LA-3); (**G**) contact between the limonitic, brecciated zone, and medium bedded algal mat dolomite; (**H**) snow white, brecciated quartzite (LA-4); (**I**) composite unconformity between the brecciated quartzite of the Abbottabad Formation and the Hangu Formation.

The following four lithofacies were observed in the field (Table 1).

4.1.1. Dolomite Member (LA-1)

The dolomite member can be separated into two zones. Figure 5B shows fine-grained, light grey to cream grey dolomite with cherty bands in the basal zone. Dolomite is thin to medium-bedded, highly jointed and fractured, hard, compact, fine grained, and cherty in general. Chert is found as grey to dark grey layers, patches, and lenses. Dolomite is brittle and fractures into small, angular fragments due to the presence of silica. The upper zone is composed of thinly bedded grey to dark grey dolomite with blackish shale (Figure 5C). This zone extends from 0 to 205 m above the ground (Figure 4).

4.1.2. Stromatolitic Dolomite Member (LA-2)

This is a fine-grained dolomite zone, with thinly laminated algal mats (Figure 5D) to thick, dome-shaped growing stromatolites (Figure 5E).

The color of dolomite is light gray with chert bands. Stromatolites are most common in the study area as stacked hemispheroids (SH) that form columns separated by sediment (Figure 5E) [38]. The laminae domes have varying widths (subtypes SH-C and SH-V). Even though the region experienced periodic storm activity, low energy conditions prevailed. Tidal flat conditions occurred in general throughout the formation of the investigated sequence. This zone is around 200 m thick and displays a gradual increase in water depth (Figure 4).

4.1.3. Oxidized, Ferruginous Dolomite Member (LA-3)

An oxidized zone can be seen in the central part of the stromatolitic dolomite facies (Figure 5F). This zone is greenish-reddish brown, rusty stained, brecciated, and highly limonitic. This zone is 16.2 m thick at Yadgar section (Monument Point) and extends more than 100 m along the dip and strike (Figure 5G). The zone is characterized by shearing and considerable silicification. Quartz lenses are found in phyllitic-looking altered rocks (Figure 4).

4.1.4. Quartzite (Quartzose Sandstone) Member (LA-4)

In the study area, quartzite rests on top of stromatolitic dolomite. This quartzite is fine-grained, white to snow white, with brownish to yellowish encrustations on the joints (Figure 5H). The quartzite ranges in thickness from 9 to 25 m, is brecciated at the top, and is unconformably overlain by bauxite from the Hangu Formation (Figure 5I). This zone extends from 410 to 438 m above the LA-2 facies (Figure 4).

4.1.5. Microfacies of the Abbottabad Formation

The petrographic analysis of 30 dolomite samples revealed different grain types, such as ooids, pellets, intraclasts, and the remains of unidentified fossils (Figures 6–9). The lower part of the Abbottabad Formation has fine crystalline dolomite, but the upper part is entirely quarzitic and brecciated. Dominant microfacies include those composed of dolomite, chert, chalcedony, various types of bioclasts, and quartz, with textures ranging from crystalline to grain stone. Five microfacies have been identified and are listed below.

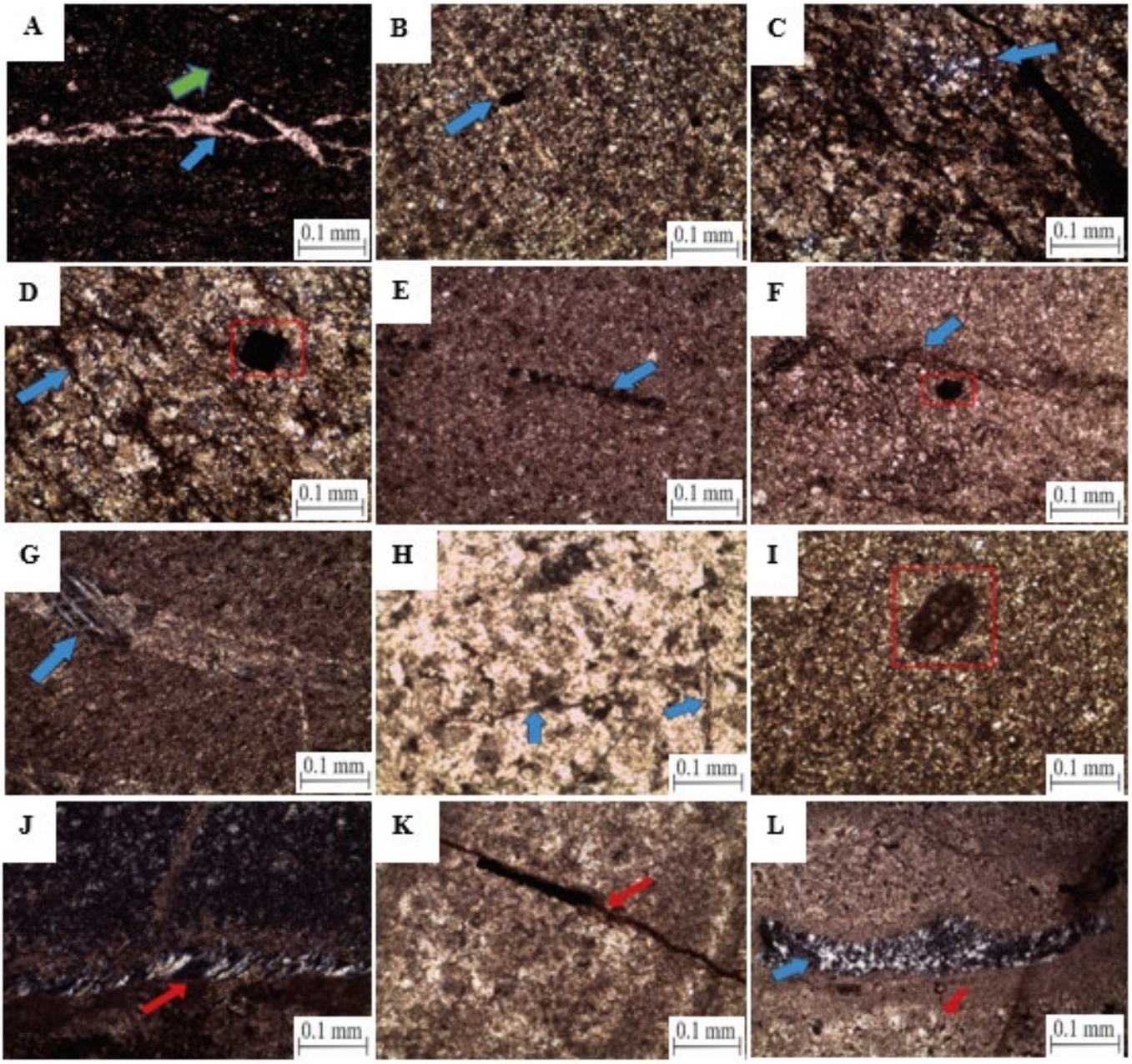

Figure 6. Photomicrographs of the Dol. I microfacies of the Abbottabad Formation. (**A**) Partially dolomitized vein (blue arrow) and carbonaceous material in fine dolomite rhombs (green arrow) (KA-1; PPL. 10×). (**B**) Fine equigranular, planar-s dolomite facie and pyrite grains upon dolomite vein (blue arrow) (KA-2; XPL. 10×). (**C**) Fine crystalline dolomite with chalcedony (blue arrow) (KA-3; XPL. 10×). (**D**) Stylolite veins highlighted by hematite (blue arrow) and rectangle showing cubic pyrite in planar dolomite facie (KA-3; XPL. 10×). (**E**) Bioclast in fine crystalline dolomite (blue arrow) (KA-4; PPL. 10×). (**F**) Stylolite vein (blue arrow) and rectangle showing hematite grain (KA-4; PPL. 10×). (**G**) Calcite and dolomite vein (blue arrow) in fine crystalline dolomite (KA-19; XPL. 10×). (**H**) Bioclasts in fine crystalline dolomite (blue arrows) (KA-27; XPL. 10×). (**I**) Bioclast in fine crystalline dolomite (KA-31; PPL. 10×). (**J**) Chalcedony vein (red arrow) and chert in dolomite (KA-37; XPL. 10×). (**K**) Hematite vein in dolomite (KA-37; XPL. 10×). (**L**) Chalcedony patches (blue arrow), and chert (red arrow) in fine planar-s dolomite (KA-44; XPL. 4×).

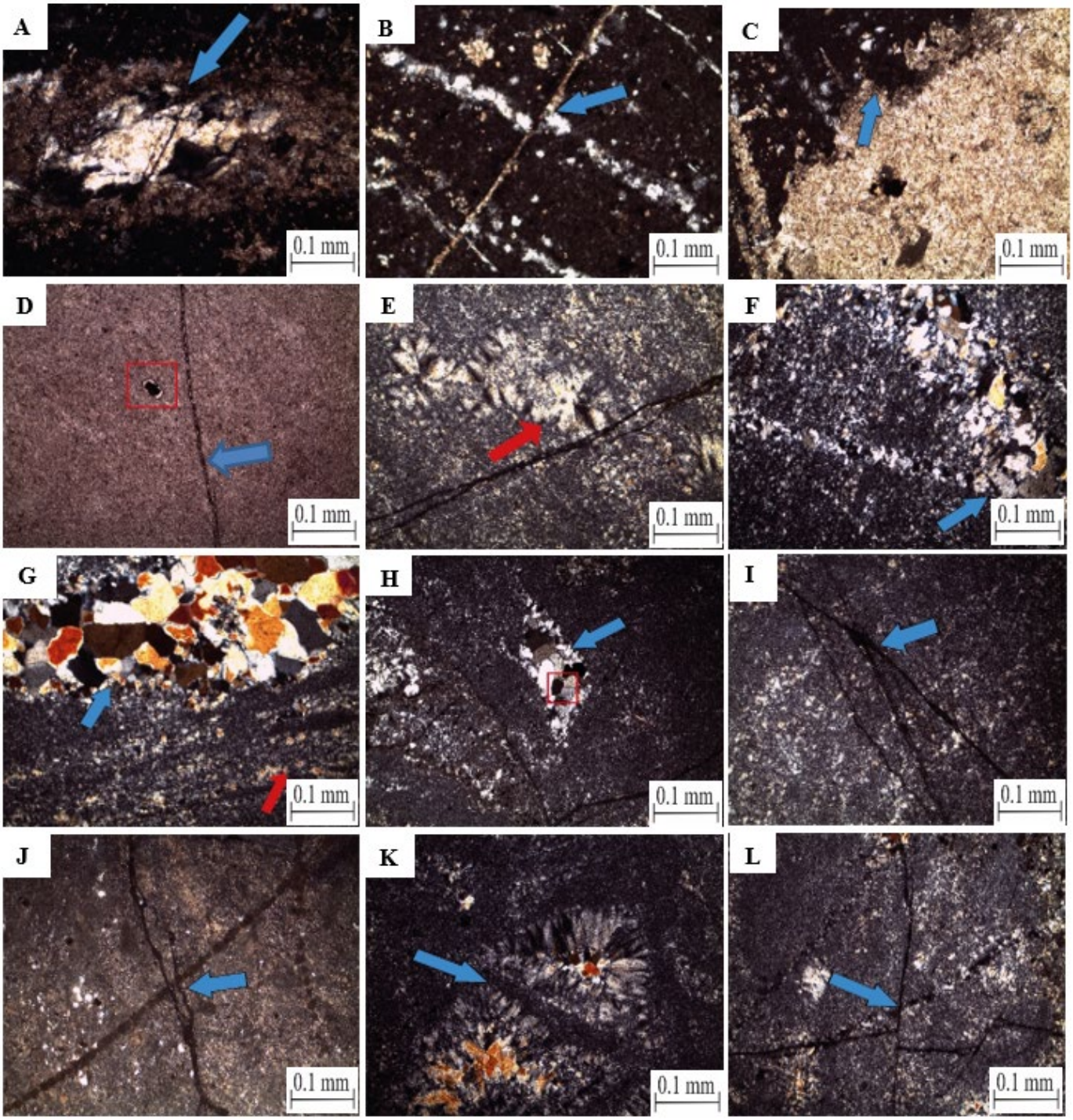

Figure 7. Photomicrographs of the Dol. II microfacies of the Abbottabad Formation. (**A**) Chert inclusion in dolomite vein (blue arrow) of cherty dolomite (KA-5; PPL. 10×). (**B**) Dolomite vein cutting chalcedony (blue arrow) (KA-5; XPL. 10×). (**C**) Irregular contact of dolomite and chert (blue arrow) (KA-5; XPL. 10×). (**D**) Dolomitized veins highlighted by hematite (blue arrow) and rectangle showing apatite (KA-41, PPL. 4×). (**E**) Chalcedony (red arrow) and hematite vein (KA-41; XPL. 4×). (**F**) cross cutting cherty veins (blue arrow) in cryptocrystalline silica (KA-41; XPL. 4×). (**G**) Microcrystalline (red arrow) and cryptocrystalline chert (blue arrow) (KA-41; XPL. 4×). (**H**). Chert nodule (blue arrow) containing pyrite (KA-59; XPL. 4×). (**I**) Hematite veins (blue arrow) in microcrystalline silica (KA-59; XPL. 4×). (**J**) Hematite veins cut by bioclast (KA-60; XPL. 4×). (**K**) Chalcedony (blue arrow) (KA-61; XPL. 4×). (**L**) Unfilled veins showing micro faults (blue arrow) (KA-61; XPL. 4×).

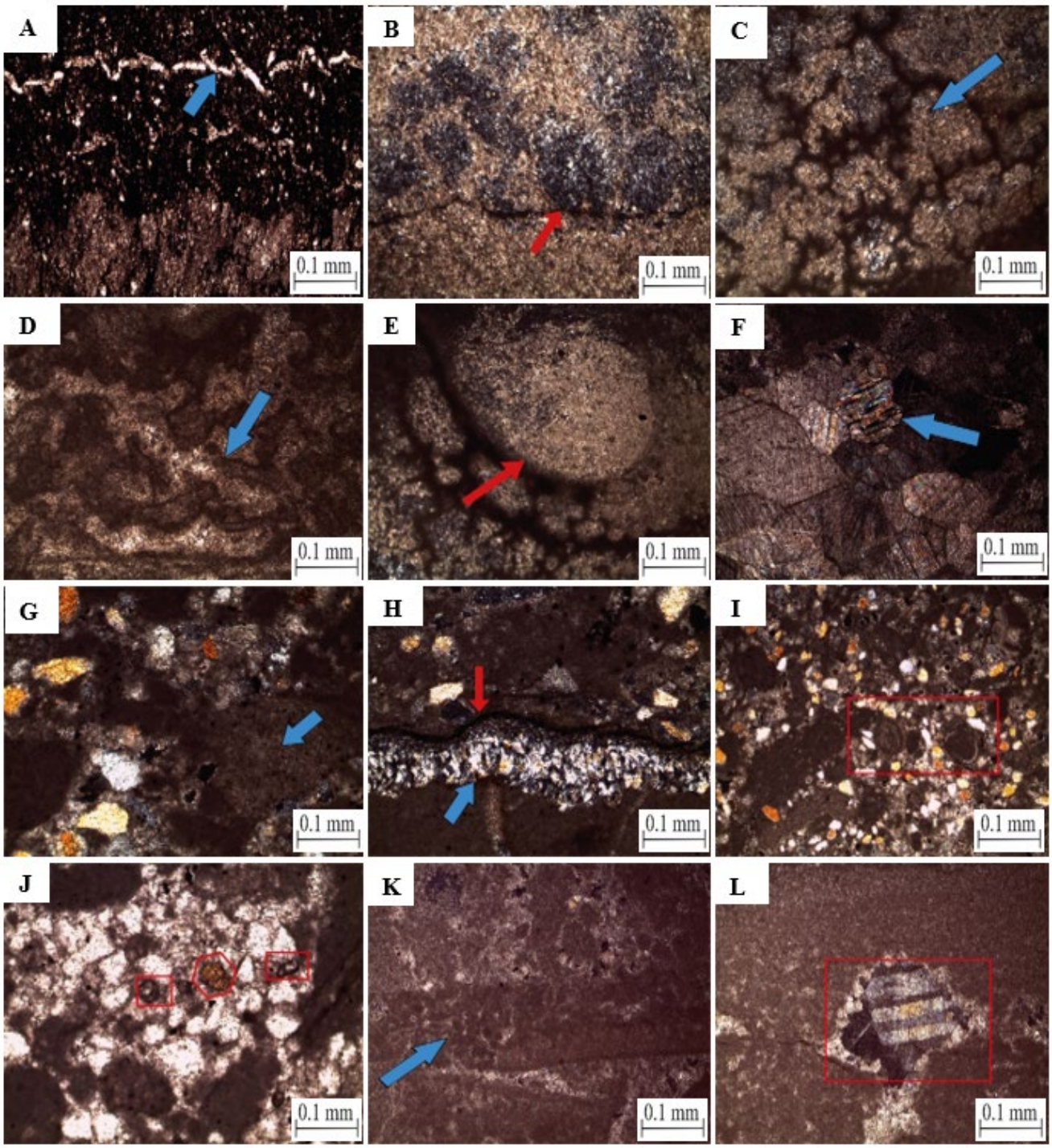

Figure 8. Photomicrographs of the Dol. III microfacies of the Abbottabad Formation. (**A**) Microbial lamination (blue arrow) and organic matter (KA-8; PPL. 4×). (**B**) Chert patches with stylolite vein (red arrow) (KA-35; XPL. 4×). (**C**) Algae bioclast (blue arrow) (KA-56; XPL. 4×). (**D**) Dolomitized algal mats (KA-56; XPL. 4×). (**E**) Dolomitized algae bioclast (red arrow) (KA-56; XPL. 4×) (**F**) Spary calcite (blue arrow) (KA-56; XPL. 4×). (**G**) Algal mats (blue arrow) partially dolomitized (KA-63; XPL. 10×). (**H**). Chalcedony vein (blue color) and hematite vein (red arrow) along algal mats (KA-63; XPL. 10×). (**I**) Rectangle showing pellets (KA-63; XPL. 4×). (**J**) Rectangle showing zircon and polygon showing tourmaline crystals (KA-63; XPL. 10×). (**K**) Algal mat (blue arrow) (KA-67; XPL. 4×). (**L**) Rectangle showing cavity filled by calcite and then dolomitized (KA-67; XPL. 4×).

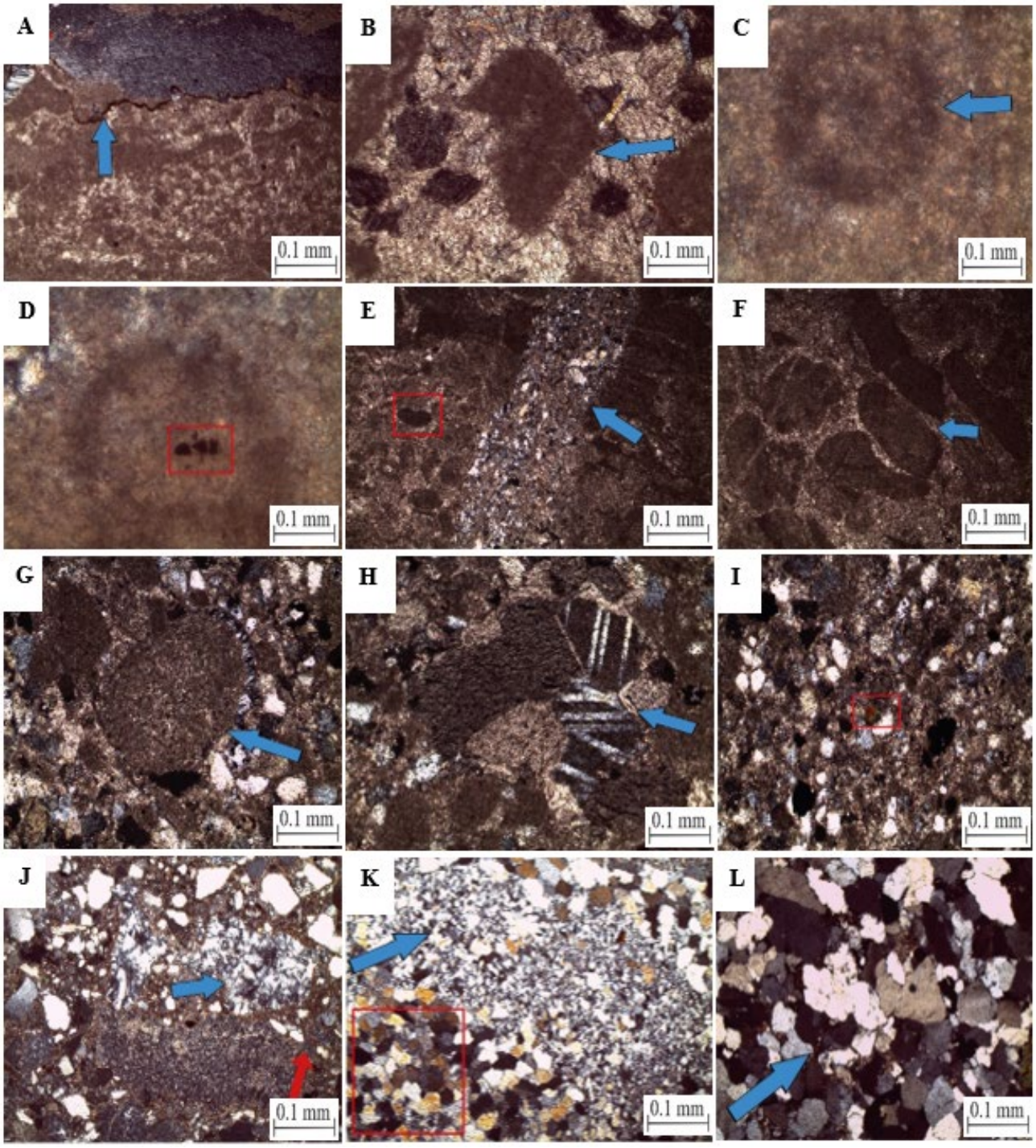

Figure 9. Photomicrographs of the Dol. III, IV and arenite microfacies of the Abbottabad Formation. (**A**) Chert (red arrow) and stylolite vein (blue arrow) along algal mats in Dol. III facies (KA-67; XPL. 4×). (**B**) Bioclast (blue arrow) in Dol. III facies (KA-67; XPL. 10×). (**C**) Dolomitized ooid (blue arrow) in Dol. III facies (KA-70; XPL. 40×). (**D**) Pyrite grains in bioclast in Dol. III facies (KA-70; XPL. 40×). (**E**) Cherty and dolomitic vein and rectangle showing pellets in Dol IV facies (KA-50; XPL. 4×). (**F**) Intraclasts (blue arrow) in Dol IV facies (KA-50; XPL. 4×). (**G**) Dolomite clast (blue arrow) in Dol IV facies (KA-65; XPL. 10×). (**H**). Spary calcite (blue arrow) in Dol IV facies (KA-65; XPL. 10×). (**I**). Tourmaline crystal (red rectangle) in Dol IV facies (KA-65; XPL. 10×). (**J**). Chalcedony (red arrow) and chert (blue arrow) in Dol IV facies (KA-76; XPL. 4×). (**K**). Chert (blue arrow) and quartz (red rectangle) in arenite facies (KA-82; XPL. 4×). (**L**). Sub-angular, sutured grains of quartz in arenite facies (KA-87; XPL. 4×).

4.1.6. Fine Crystalline Dolomite (Dol. I)

In the Kamsar section, ten samples (KA-1, KA-2, KA-3, KA-4, KA-19, KA-22, KA-27, KA-31, KA-37, and KA-44; Table 2) are microcrystalline to fine-crystalline dolomite (Dol. I). Around 70% to 95% of this microfacies are composed of dolomite, which has a nonplanar to planar texture (Figure 6A–C).

Dolomite crystals are compacted, subhedral, and are of the same size. Chert, which is composed of small fibers of silica, is between 1% and 5% (Figure 6C,J,L), and pyrite, which is a Fe-rich residue, is also between 1% and 5%. Pyrite is observed in both cubic (Figure 6D) and framboidal (Figure 6F) shapes, which formed during deposition and diagenesis, respectively. Bioclasts from the Cambrian period are between 1% and 2% (Figure 6E,H). Dolomitized bioclast in fine crystalline dolomite is present (Figure 6I). This microfacies also has stylolite veins (Figure 6D,F), chalcedony veins (Figure 6I,J), a hematite vein (Figure 6K), and calcite and dolomite veins (Figure 6G). Chemical compaction occurs in many sediments. This is shown by pressure solutions and the formation of stylolites [40]. Load and/or tectonic stress can cause pressure to build up. Based on the Sibley and Gregg [34] textural classification, the Dol. I microfacies of the study area are crystalline planar-s to planar-e type dolomite, most of which is dolomite replacing other sediments.

4.1.7. Dolomitic Cryptocrystalline Chert (Dol. II)

Dolomitic cryptocrystalline chert was observed in seven samples (KA-5, KA-41, KA-59, KA-60, KA-61, KA-68, and KA-84; Tables 2 and 3) (Dol. II). Petrographically, this microfacies has between 5% and 30% dolomite with planar-c texture (Figure 7A). In this microfacies, the amount of silica is very high, and it is visible in the form of chert, which is a fine-grained sedimentary rock made of microcrystalline or cryptocrystalline quartz (SiO2) and chalcedony. Chert is between 5% and 60% (Figure 7C,F,H), cryptocrystalline silica is between 30% and 65% (Figure 7F,G), and chalcedony is between 8% and 24% (Figure 7B,E,K). The lower part of this facies (KA-5) is in a transitional phase, and the middle and upper parts have more silica. Grains of apatite (Figure 7D) and pyrite (Figure 7H) are also observed.

4.1.8. Dolomite with Algal Mats (Dol. III)

These facies were observed in eight samples (KA-8, KA-35, KA-56, KA-63, KA-66, KA-67, KA-69, and KA-70; Tables 2 and 3) (Dol. III). The quantity of dolomite in this microfacies ranges from 18% to 78% and shows a non-planar-c type texture. Algal mats are presented as a sedimentary structure along carbonaceous material, ranging from 5–55%. The thickness of the micritic laminae is variable (Figure 8A,D,G). These crusts, which are several centimeters thick, are thought to be carbonate precipitation due to micro-organisms. Thin sections of studied stromatolites show that they are composed of a fine-grained sediment that is well-laminated. This is because fine-grained sediment was deposited in small amounts at different times and was then trapped (Figure 8B,C,K). The iron minerals, such as hematite, in the dark microbial laminae of stromatolites (Figure 8A,H) are present. Chert is between 4% and 30% (Figure 9A). There are also partially dolomitized bioclast (Figure 8B) and peloids (Figure 9C,D) in this microfacies.

4.1.9. Intraclastic–Dolo-Grain Stone (Dol. IV)

Three samples (KA-50, KA-65, and KA-76; Tables 2 and 3) are intraclast dolo-grain stone (Dol. IV). Dolomite makes up between 20 and 25% of this microfacies, revealing planar idiotopic (Planar-p). In this microfacies, intraclasts of different types of rock, such as dolomite, chert, and carbonaceous material, are common and constitute 5–60% (Figure 9F,G), and chert makes up 5–25% (Figure 9E,J).

4.1.10. Fine Quarzitic Arenite

Two samples. (KA-82 and KA-87; Table 3) are arenites. The quartz amount in this microfacies is around 95%. Quartz grains are moderately sorted and sutured (Figure 9K,L).

4.1.11. XRD and EDX Analysis of Dolostone

The XRD analysis of dolomite indicates similar mineral composition as determined through petrographic studies. The main minerals found in dolostone are dolomite (26–68%), calcite (5–47%), quartz/chert/moganite (13–66%), pyrite (up to 3%), and carbonaceous material (up to 5%). The XRD analysis of dolostone further reveals that dolomite mineral decreases from base to top and chert increases towards top (Figure 10A–D).

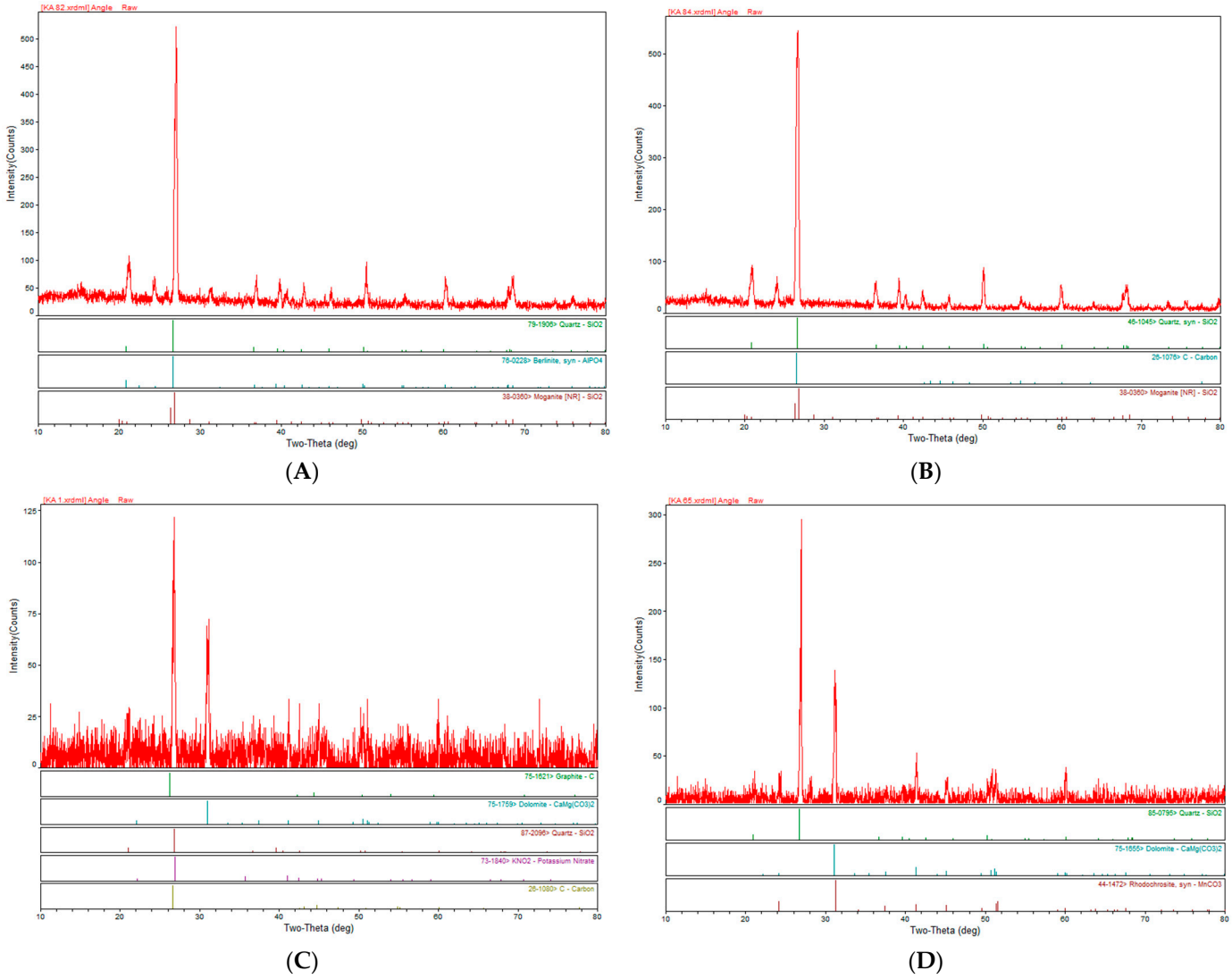

Figure 10. XRD pattern of the Abbottabad Formation. (**A**) Fine crystalline dolomite (LA-1; Dol. I; sample no. KA-1); (**B**) dolomite (LA-3; Dol. IV; sample no. KA-65); (**C**) quartzite (LA-4; arenite microfacies; sample no. KA-82); (**D**) dolomite (LA-1; Dol. II; sample no. KA-84).

The diffractogram A of Dol. I microfacies (sample no. KA-1) demonstrates the presence of dolomite, carbonaceous material, potassium nitrate (KNO_3), and quartz (Figure 10A). The occurrence of potassium nitrate in the Dol. I microfacies probably indicates that the rocks have been altered by the actions of microorganisms, such as bacteria or fungi, which produce nitrate as a byproduct of their metabolic processes. Diffractogram B of Dol. IV microfacies (sample no. KA-65) shows the presence of dolomite, quartz, and rhodochrosite (Figure 10B). The presence of rhodochrosite ($MnCO_3$) in dolomite indicates a hydrothermal alteration or replacement of the original dolomite. Diffractogram C of arenite microfacies (sample no. KA-82) shows the presence of quartz; berlinite ($AlPO_4$), which is a high-temperature hydrothermal or metasomatic phosphate mineral; and moganite (Figure 10C).

Diffractogram D of Dol II shows the presence of quartz (SiO_2), carbonaceous material (C), and moganite (SiO_2) (Figure 10D). However, no dolomite mineral was observed in this diffractogram. The dolomite mineral was replaced by quartz and moganite during metasomatism. In the Dol. II microfacies, hydrothermal solutions played vital role in replacing dolomite during metasomatism. In the field, this Dol. II microfacies was undifferentiated due to the preservation of the original texture of the dolomite. Texturally, Dol. II was similar to LA-1 lithofacies.

The elemental analysis of dolostone through EDX determined the major elements in weight percent and atomic percent. The weight percent of elements found in different facies of dolostone are carbon (up to 12%), oxygen (31–56%), magnesium (up to 9%), aluminum (up to 4%), silicon (2–64%), calcium (up to 53%), potassium (up to 6%) iron (up to 7%), and sulfur (up to 3%) (Table 4). These different elements constitute the minerals that found in the dolostone as confirmed by petrographic and XRD analysis.

Table 4. Energy dispersive X-ray (EDX) percentage of elements present in samples of the Abbottabad Formation.

Sample No.	Elements Weight%									Elements Atomic%								
	C	O	Mg	Al	Si	Ca	K	Fe	S	C	O	Mg	Al	Si	Ca	K	Fe	S
KA-3	0.94	52.30	4.12	4.13	24.93	5.90	5.55	2.17	–	0.85	67.21	3.49	3.45	18.26	3.03	2.92	0.8	–
KA-8	0.39	47.05	0.65	0.37	2.42	47.72	1.40	–	–	0.76	67.97	0.62	0.31	1.99	27.52	0.83	–	–
KA-22a	0.33	55.80	1.37	1.33	5.36	33.73	2.08	–	–	0.58	74.10	1.20	1.05	4.06	17.88	1.03	–	–
KA-22b	0.81	54.07	4.80	4.13	13.31	14.53	4.25	–	–	1.40	70.17	4.10	3.18	9.84	7.53	2.26	–	–
KA-27	12.36	31.02	0.55	0.27	2.70	52.71	0.39	–	–	23.27	43.85	0.51	0.22	2.17	29.74	0.23	–	–
KA 60	–	31.91	–	2.99	51.32	–	3.41	7.40	2.98	–	46.98	–	2.61	43.05	–	2.05	3.12	2.2
KA 61		33.48			64.29			2.23			47.32			51.77			0.90	
KA 67	14.66	32.13	9.26	2.21	9.94	28.60	2.15	1.06		25.25	41.55	7.88	1.70	7.32	14.76	1.14	0.39	

Overall, the Cambrian dolostone of the Abbottabad Formation mainly comprised dolomite mineral ($CaMg(CO_3)_2$), with chert (SiO_2), calcite ($CaCO_3$), Pyrite (FeS_2), and carbonaceous material (C). Trace amounts of zircon ($ZrSiO_4$) and muscovite ($KAl_2(AlSi_3O_{10})(F,OH)_2$,) were also found in the dolostone of the Abbottabad Formation (Figure 8; Table 3).

5. Discussion

5.1. Regional Stratigraphic Correlations

Early Cambrian rocks are exposed in various locations in the northern Pakistan, including the Salt Range [28,41], Peshawar Basin [42], Abbottabad [43,44], Muzaffarabad, and Kotli [15,45,46]. The Cambrian Ambar Formation in the Peshawar basin is a possible equivalent of the Abbottabad Formation [47]. Latif [48] classifies the Abbottabad Group into Sirban and Kakul formations. The Kakul Formation is divided into four members: the Tanakki Conglomerate, the Sangargali Member, the Mahmdagali Member, and the Mirpur Sandstone. In the Abbottabad region, Qasim, Khan and Haneef [44] divided the Abbottabad Formation into three distinct units: (1) the base arenaceous unit, (2) the intermediate dolomite unit, and (3) the upper quartzite unit. In contrast to the Hazara region, the Abbottabad Formation in the studied area lacks the lower arenaceous member and stromatolitic-dolomitic unit, which are exclusively visible in the Muzaffarabad region. Hazara's Abbottabad Formation is associated with two lithofacies, LA-1 and LA-4, while the LA-1 of the study area is correlated with the Cambrian Jutana Formation of Potwar/Salt Range only [22]. The main difference is the absence of stromatolitic unit in the Salt Range and the Abbottabad area compared to the Muzaffarabad area. It is worth mentioning that in the Salt Range, the Cambrian rocks are present in the Precambrian Salt Range Formation instead of the Hazara Formation (Abbottabad area) or the Dogra Formation (Muzaffarabad area).

5.2. Dolomite Texture and Mechanism of Dolomitization

Heterogeneous textures were observed in the Cambrian dolomite. The texture of the dolomite varies from base to top and correspond to four microfacies of the dolomite, i.e., fine crystalline dolomite (Dol. I), dolomitic cryptocrystalline chert (Dol. II), dolomite with algal mats (Dol. III), and intraclastic-dolo-grain stone (Dol. IV). The texture of the Dol. I microfacies is non-planar xenotopic to planar e and planar s, where dolomite crystals are tightly packed anhedral to euhedral. Planar subhedral to euhedral replacive dolomite crystals formed in the early diagenesis stage (Figure 11). The Dol-I microfacies is present as fine-grained rhombohedral crystals and indicates that the dolomitization process was slow and controlled by kinetic constraints. The texture of the Dol. II microfacies is planar c type, in which pores are filled by micro crystalline to crypto crystalline chert. The addition of this silica occurred through the replacement of dolomite crystal during the syndiagenetic–epigenetic period. The large amounts of silica were provided in the Proto-Tethys Ocean by the hydrothermal fluids, and this silica replaced the dolomite selectively. Selective metasomatism was probably caused by the weak acidic environment due to the decomposition of organic matter, which is beneficial for the deposition and metasomatism of silica (Figure 11). The texture of the Dol. III microfacies is the non-planar c type, where a scimitar-like termination has been observed between algal mats dolomite crystals and non-algal mats dolomite. Non-planar dolomite can form at low temperatures, under conditions of high supersaturation, although such occurrences are fairly rare (Figure 11). The texture of the Dol. IV microfacies is the planar p (porphyrotopic) type, where dolomite crystals are embedded in a calcite matrix. The porphyrotopic planar dolomite probably formed in peritidal environments through reflux dolomitization. Based on the petrography it seems as though Dol. IV was dolomitized than eroded and deposited. This suggests early dolomitization. Additionally, dolomitization occurred prior to the regression at least in some places on the dip of this site. During the regression, it was subsequently eroded and transported, at which point dolomitization could have also been enhanced. The presence of detrital grains (tourmaline, quartz, zircon, and apatite) with intraclasts of dolomite also support this phenomenon.

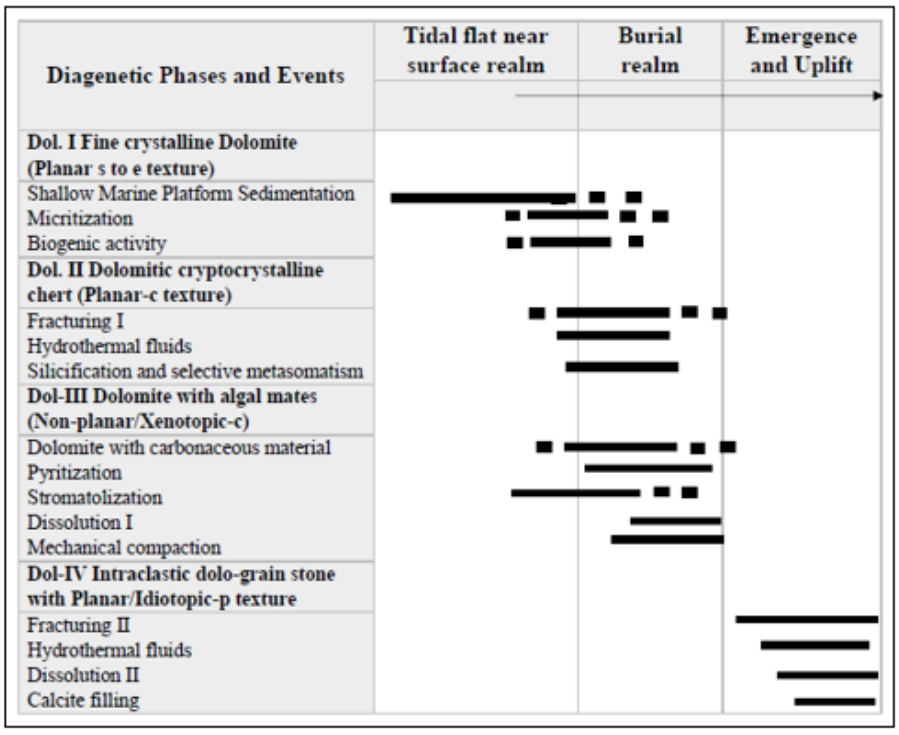

Figure 11. Paragenetic history of the dolomite of the Abbottabad Formation, representing early tidal flat period followed by s burial period and uplift.

Dolomitization is a replacement reaction, whereby Mg replaces Ca in the crystal lattice. This is dictated by hydrogeological mechanisms as well as thermodynamic and kinetic factors [45–47]. Dolomitization is often the product of early diagenetic processes in carbonate-rich mud or limestone, while it is the result of a higher grade of dolomitization in solid limestone [49–51]. In the Upper Indus Basin (UIB), above the Precambrian crystalline basement, the Salt Range Formation comprises thick reserves of salt. The thickness of these deposits provides a thread of a lagoonal environment [41]. The Cambrian-aged Abbottabad Formation in the Proto-Tethys Ocean overlies the older salt-related paleolatitudes. The sedimentological hierarchy of facies presents an intricate picture of the depositional history of geological strata. A careful analysis of this hierarchy reveals that the episodic regressive events have played a significant role in shaping the depositional environment. Specifically, these events have given rise to a horizon where limestone was deposited in a shallow intertidal to subtidal environment. Furthermore, this limestone was subsequently subjected to dolomitization, either via penecontemporaneously or through reflux mechanisms (Figure 12). The presence of a significant amount of silica and silicate in the Dol I and Dol II suggests that there were high concentrations of silica in the solution during dolomite formation. Recent studies have shown that dissolved silica could promote primary dolomite formation with silica adsorbed onto carbonate surfaces, which transforms either to authigenic clay or chert/chalcedony during burial [52,53].

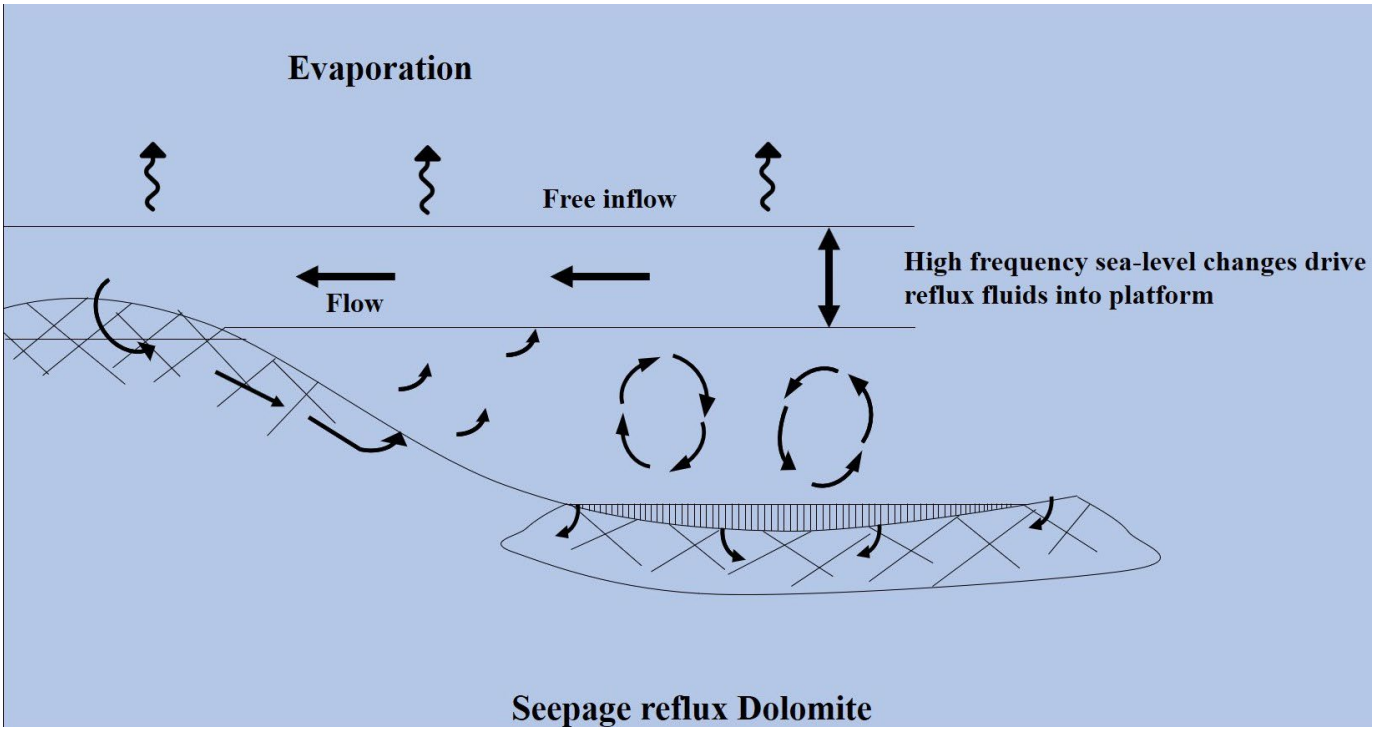

Figure 12. Mechanism of dolomitization (modified after [54,55]).

5.3. Depositional Environment and Proto-Tethys Evolution

In the studied area, a non-conformity indicates the top of the Precambrian Dogra slates and the fine crystalline dolomite is followed by shale. The overall succession of this lithofacies (LA-1) from base to top demonstrates an upward coarsening trend: from shallow subtidal dominated units to supratidal dominated units (Figure 4). The coarsening upward sequence in carbonate rocks can be recognized in the sediment layers as it become thicker as it rises and displays diagenetic features, such as cementation and dissolution, which are more common in the coarser upper part of the sequence. Above the LA-1, stromatolitic dolomites (LA-2) contain fenestrae, microbial laminae, and chert lenses, which are characteristic of shallow subtidal to supratidal settings [56]. This stage is characterized

by the deposition of microbial dolomite before a major base-level decrease (Figure 13). Stromatolites vary in size and form in these facies. Stromatolites are laminated, arched organic sedimentary formations produced by blue-green algae that adhere to sediment (cyanobacteria). Bacteria precipitate, trap, and bind sediment layers to create accretionary structures. This appears as domes, conical, or complexly branched structures ranging in size from a little finger to a house. In this lithofacies, both cubic and framboidal pyrite (FeS_2) were found as syngenetic to diagenetic grains, respectively [13,57]. These grains can form in low-temperature diagenetic environments or precipitate in anoxic waters. They are typical minerals found in organic-rich sediments and indicate euxinic depositional conditions [58]. These euxinic conditions occurred when water was both anoxic and sulfidic. Oxidized, ferruginous, and limonitic dolomite (LA-3) characterized surface karstification products as well as karstic depression fills, revealing a hundred million years of exposure. Numerous studies of modern and ancient karst features indicate that the most favorable conditions for prominent karstification are moderate to high rainfall [59] and relatively pure, dense, and thick carbonate rocks with appropriate conduits, such as fractures, joints, faults, or selective solutional pipes [60–62]. In the Kamsar section, the quartzite unit (LA-4) is composed of medium- to fine-grained sandstone and brecciated sandstone at the top; these characteristics indicate the subaerial exposure (Figure 13).

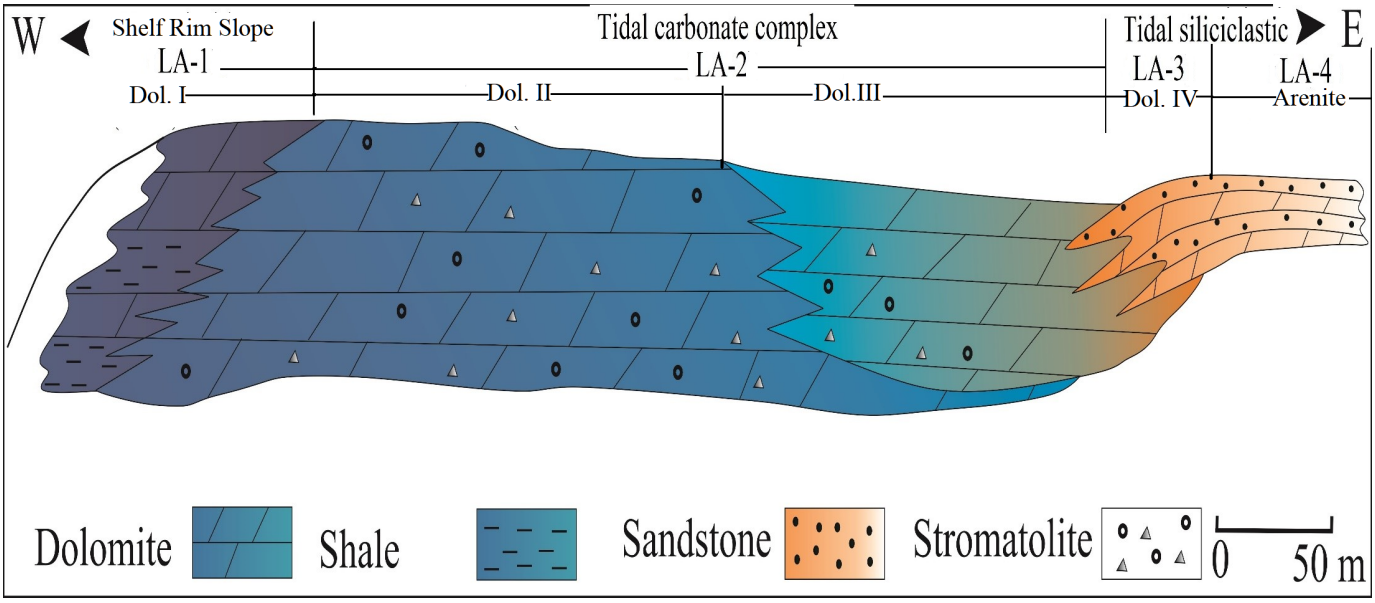

Figure 13. Depositional model showing the lateral facies distribution of the Abbottabad Formation from west (**left**) to east (**right**).

The presence of various types of dolomites, chert, and quartz in thin sections also aided in the petrographical investigation of the depositional phenomenon. During the process of diagenesis, the silica in sediments change from opal to microcrystalline quartz in mature chert [63]. Silica mobilized from hydrothermal fluids and clay minerals might potentially contribute to silicification [64]. Petrographic studies helped in delineating four phases of distinct characteristic features. These include fine crystalline dolomite (Dol. I), dolomitic crystalline chert (Dol. II), dolomite with algal mats (Dol. III), and intraclastic dolo-grain stone (Dol. IV) (Figure 11).

An initial phase of dolomite (Dol. I) resulted from interaction with Mg-rich fluids originated during earliest diagenetic phase, representing penecontemporaneous or reflux mechanism during early Cambrian. This was followed by an increase in different types of silica (Dol. II) from hydrothermal fluids and the growth of stromatolites/algal mats (Dol. III). Dol. II and Dol. III are associated with subtidal to supratidal conditions, whereas Dol. IV formation is associated with sub-aerial exposure or orogenic events. In

general, the available data indicate that dolomitization resulting from reflux mechanisms can be identified in thin sections by the occurrence of saddle-shaped dolomite crystals, a coarse-crystalline texture, the replacement of previously formed minerals, the selective dolomitization of certain rock fabrics, and atypical crystallographic orientations.

The Proto-Tethys Ocean existed on the Earth between 550–330 mya [65]. The Proto-Tethys Ocean was highly susceptible to evaporitic conditions during the Late Precambrian, which resulted in the deposition of salt basement over a broad region in the Upper Indus Basin (UIB) [37]. These sediments comprise the Precambrian Salt Range Formation. The Muzaffarabad region of the Kamsar section is located on the Proto-Tethys Ocean's passive margin. The sedimentological hierarchy of facies indicates that the episodic regressive events provide a horizon where limestone was deposited in shallow intertidal to subtidal environment and later subjected to dolomitization penecontemporaneously or via a reflux mechanism (Figure 12). Based on the observed data, it can be stated that during regression events and increasing restriction, both temperature and salinity tend to increase. Overall, the combination of kinetic, geochemical, and biological factors initiates dolomitization depending on the specific geological setting and local conditions. Additionally, if evaporites precipitate, there is a likelihood of an increase in the Mg:Ca ratio [66]. These kinetic conditions collectively facilitate penecontemporaneous dolomitization [67].

6. Conclusions

The following results were obtained based on field observations, facies analysis, petrographic, and geochemical studies:

1. The Abbottabad Formation lithologically consists of fine crystalline dolomite (LA-1), microbially laminated dolomite (LA-2), oxidized, ferruginous dolomite (LA-3), and quartzite (LA-4), corresponding to four microfacies, i.e., fine crystalline dolomite (Dol. I), dolomitic cryptocrystalline chert (Dol. II), dolomite with algal mats (Dol. III), and intraclastic dolo-grain stone (Dol. IV).
2. Stromatolites are often composed of vertically stacked hemispheroids that are subordinated by laterally linked hemispheroids. In general, conditions suggestive of tidal flats existed throughout the formation of this sequence.
3. The overall succession of the Abbottabad Formation from base to top demonstrates a coarsening trend succession, indicated by the sediment layers becoming thicker as they rise and cementation and dissolution being more common in the upper part of the sequence. This succession represents shallow subtidal units becoming supratidal-dominated units. Oxidized, limonitic dolomite (LA-3) represents surface karstification products, whereas brecciated quartzite (LA-4) denotes subaerial exposure.
4. The X-ray diffraction (XRD) analysis of dolomite revealed a mineral composition consistent with that determined by petrographic studies, with dolostone containing primarily dolomite, calcite, quartz/chert/moganite, potassium nitrate (KNO_3), rhodochrosite ($MnCO_3$), berlinite ($AlPO_4$), and minor amounts of pyrite and carbonaceous material and shows the dolomite mineral decreasing from base to top, while chert increases towards the top.
5. The EDX analysis determined the weight percent of different elements, such as carbon, oxygen, magnesium, aluminum, silicon, calcium, potassium, iron, and sulfur. These elements constitute the minerals that found in the dolostone as confirmed by petrographic and XRD analysis.
6. The Dol. I microfacies is characterized by non-planar xenotopic texture, with tightly packed anhedral to euhedral dolomite crystals formed in the early diagenesis stage, indicating slow and controlled dolomitization. Dol. II microfacies has a planar-c type texture with pores filled by micro to crypto crystalline chert, formed by the selective replacement of dolomite by silica. The abundance of silica in the Proto-Tethys Ocean was due to hydrothermal fluids. The Dol. III microfacies shows non-planar-c type texture, where scimitar-like termination is observed between algal mats and non-algal mats dolomite. Dol. IV microfacies exhibits a planar-p (porphyrotopic) texture,

where dolomite crystals embedded in a calcite matrix probably formed in peritidal environments through reflux dolomitization.

7. The sedimentological hierarchy of facies indicates that the episodic regressive events provide a horizon where limestone was deposited in the shallow intertidal to subtidal environment and later subjected to dolomitization penecontemporaneously or via a reflux mechanism.
8. Overall, the evidence of reflux dolomitization in thin sections includes the presence of saddle-shaped dolomite crystals, coarse-crystalline texture, the replacement of earlier-formed minerals, fabric-selective dolomitization, and unusual crystallographic orientations.

Author Contributions: Conceptualization, S.K.A., R.A.L. and A.G.S.; methodology, S.K.A., T.M. and M.S.M.; software, S.K.A., H.T.J. and A.B; validation, S.K.A., G.K. and H.T.J.; formal analysis, M.S.M. and S.K.A.; investigation, S.K.A., H.T.J., R.A.L., A.G.S., T.M., G.K. and A.B.; resources, S.K.A.; data curation, S.K.A., H.T.J., G.K. and M.S.M.; writing—original draft preparation, S.K.A.; writing—review and editing, S.K.A., H.T.J., M.S.M., T.M., G.K., A.B. and K.U.M.; visualization, S.K.A., M.S.M., H.T.J. and K.U.M.; supervision, R.A.L., A.G.S. and T.M.; project administration, R.A.L., S.K.A., G.K. and H.T.J.; funding acquisition, G.K. All authors have read and agreed to the published version of the manuscript.

Funding: This research received no external funding.

Institutional Review Board Statement: Not applicable.

Informed Consent Statement: Not applicable.

Data Availability Statement: The data used in this work are available on request from the corresponding author(s).

Acknowledgments: We are thankful to the Muhammad Sabir Khan, Shahab Pervez, Mirza Shahid Baig, Muhammad Basharat, Tayyab Riaz, and the Director of the Institute of Geology, University of Azad Jammu and Kashmir, Muzaffarabad, for their help and friendly attitudes during our research work, which was always a source of inspiration for us. Last but not the least, the authors are highly indebted to the five reviewers for their fruitful reviews, which helped us to improve the manuscript.

Conflicts of Interest: The authors declare no conflict of interest.

References

1. Bilal, A.; Mughal, M.S.; Janjuhah, H.T.; Ali, J.; Niaz, A.; Kontakiotis, G.; Antonarakou, A.; Usman, M.; Hussain, S.A.; Yang, R. Petrography and provenance of the Sub-Himalayan Kuldana Formation: Implications for tectonic setting and Palaeoclimatic conditions. *Minerals* **2022**, *12*, 794. [CrossRef]
2. Mughal, M.S.; Zhang, C.; Du, D.; Zhang, L.; Mustafa, S.; Hameed, F.; Khan, M.R.; Zaheer, M.; Blaise, D. Petrography and provenance of the Early Miocene Murree Formation, Himalayan Foreland Basin, Muzaffarabad, Pakistan. *J. Asian Earth Sci.* **2018**, *162*, 25–40. [CrossRef]
3. Bossart, P.; Dietrich, D.; Greco, A.; Ottiger, R.; Ramsay, J. A new structural interpretation of the hazara-kashmir syntaxis, Southern Himalayas, Pakistan. *Kashmir J. Geol.* **1984**, *2*, 19–36.
4. Calkins, J.A.; Matin, A.A. *The Geology and Mineral Resources of the Garhi Habibullah Quadrangle and the Kakul Area, Hazara District, Pakistan*; US Geological Survey: Reston, VA, USA, 1973; pp. 1258–2331.
5. Baig, M.; Lawrence, R. Precambrian to early Paleozoic orogenesis in the Himalaya. *Kashmir J. Geol.* **1987**, *5*, 1–22.
6. Basharat, M.; Rohn, J.; Baig, M.S.; Khan, M.R.J.G. Spatial distribution analysis of mass movements triggered by the 2005 Kashmir earthquake in the Northeast Himalayas of Pakistan. *Geomorphology* **2014**, *206*, 203–214. [CrossRef]
7. Marks, P.; Ali, C.M. The geology of the Abbottabad area, with special reference to the Infra-Trias. *Geol. Bull. Punjab Univ.* **1961**, *2*, 47–56.
8. Greco, A.J.J.G. Stratigraphy metamorphism and tectonics of the Hazara-Kashmir syntaxis area, Kash. *J. Geol.* **1991**, *8*, 939–965.
9. Baig, M.S.; Iqbal Siddiqi, M. Paleocene-Eocene Biostratirgraphy of the Yadgar Area, Muzaffarabad, Azad Kashmir, Pakistan. *Pak. J. Hydrocarb. Res.* **2006**, *16*, 59–65.
10. Khan, S.; Ahmad, W.; Ahmad, S.; Khan, J.K. Dating and depositional environment of the Tredian Formation, western Salt Range, Pakistan. *J. Himal. Earth Sci.* **2016**, *49*, 14–25.
11. Aadil, N. Stratigraphy and structure of Sarda, Manil, Changpur and Naghal areas, district Kotli, Jammu & Kashmir. *J. Geol. Soc. India* **2013**, *82*, 639–648.
12. Ashraf, M.; Chaudhry, M.; Qureshi, K. Stratigraphy of Kotli area of Azad Kashmir and its correlation with standard type areas of Pakistan. *Kashmir J. Geol.* **1983**, *1*, 19–29.

13. Bilal, A.; Yang, R.; Fan, A.; Mughal, M.S.; Li, Y.; Basharat, M.; Farooq, M. Petrofacies and diagenesis of Thanetian Lockhart Limestone in the Upper Indus Basin (Pakistan): Implications for the Ceno-Tethys Ocean. *Carbonates Evaporites* **2022**, *37*, 1–19. [CrossRef]
14. Latif, M. A Cambrian age for the Abbottabad group of Hazara, Pakistan. *Geol. Bull. Panjab Univ.* **1974**, *10*, 1–20.
15. Hussain, A.; Yeats, R.S. Geological setting of the 8 October 2005 Kashmir earthquake. *J. Seismol.* **2009**, *13*, 315–325. [CrossRef]
16. Myrow, P.M.; Hughes, N.C.; Goodge, J.W.; Fanning, C.M.; Williams, I.S.; Peng, S.; Bhargava, O.N.; Parcha, S.K.; Pogue, K.R. Extraordinary transport and mixing of sediment across Himalayan central Gondwana during the Cambrian–Ordovician. *GSA Bull.* **2010**, *122*, 1660–1670. [CrossRef]
17. Mustafa, S.; Khan, M.A.; Khan, M.R.; Sousa, L.M.; Hameed, F.; Mughal, M.S.; Niaz, A. Building stone evaluation—A case study of the sub-Himalayas, Muzaffarabad region, Azad Kashmir, Pakistan. *Eng. Geol.* **2016**, *209*, 56–69. [CrossRef]
18. Iqbal, O.; Baig, M.S.; Pervez, S.; Siddiqi, M.I. Structure and stratigraphy of Rumbli and Panjar areas of Kashmir and Pakistan with the aid of GIS. *J. Geol. Soc. India* **2018**, *91*, 57–66. [CrossRef]
19. Medlicott, H.B. Note upon the Sub-Himalayan Series in the Jammu (Jammoo) Hills. *Rec. Geol. Surv. India* **1876**, *9*, 49–57.
20. Bossart, P.; Dietrich, D.; Greco, A.; Ottiger, R.; Ramsay, J.G. The tectonic structure of the Hazara-Kashmir syntaxis, southern Himalayas, Pakistan. *Tectonics* **1988**, *7*, 273–297. [CrossRef]
21. Baig, M.S.; Yeats, R.S.; Pervez, S.; Jadoon, I.; Khan, M.R.; Sidiqui, I.; Lisa, M.; Saleem, M.; Masood, B.; Sohail, A. Active tectonics, October 8, 2005 earthquake deformation, active uplift, scarp morphology and seismic geohazards microzonation, Hazara-Kashmir Syntaxis, Northwest Himalayas, Pakistan. *J. Himal. Earth Sci.* **2010**, *43*, 17–21.
22. Khan, S.; Shah, M.M. Multiphase dolomitization in the Jutana Formation (Cambrian), Salt Range (Pakistan): Evidences from field observations, microscopic studies and isotopic analysis. *Geol. Acta* **2019**, *17*, 1–18.
23. Shah, M.M.; Nader, F.; Garcia, D.; Swennen, R.; Ellam, R. Hydrothermal dolomites in the Early Albian (Cretaceous) platform carbonates (NW Spain): Nature and origin of dolomites and dolomitising fluids. *J. Oil Gas Sci. Technol. Rev. D'ifp Energ. Nouv.* **2012**, *67*, 97–122. [CrossRef]
24. Zhang, F.; Xu, H.; Konishi, H.; Shelobolina, E.S.; Roden, E.E. Polysaccharide-catalyzed nucleation and growth of disordered dolomite: A potential precursor of sedimentary dolomite. *Am. Mineral.* **2012**, *97*, 556–567. [CrossRef]
25. Bontognali, T.R.; Vasconcelos, C.; Warthmann, R.J.; Bernasconi, S.M.; Dupraz, C.; Strohmenger, C.J.; McKENZIE, J.A. Dolomite formation within microbial mats in the coastal sabkha of Abu Dhabi (United Arab Emirates). *Sedimentology* **2010**, *57*, 824–844. [CrossRef]
26. Machel, H.G.; Lonnee, J. Hydrothermal dolomite—A product of poor definition and imagination. *Sediment. Geol.* **2002**, *152*, 163–171. [CrossRef]
27. Warren, J. Dolomite: Occurrence, evolution and economically important associations. *Earth-Sci. Rev.* **2000**, *52*, 1–81. [CrossRef]
28. Ali, S.K.; Janjuhah, H.T.; Shahzad, S.M.; Kontakiotis, G.; Saleem, M.H.; Khan, U.; Zarkogiannis, S.D.; Makri, P.; Antonarakou, A. Depositional Sedimentary Facies, Stratigraphic Control, Paleoecological Constraints, and Paleogeographic Reconstruction of Late Permian Chhidru Formation (Western Salt Range, Pakistan). *J. Mar. Sci. Eng.* **2021**, *9*, 1372. [CrossRef]
29. Kazmi, A.H.; Jan, M.Q. *Geology and Tectonics of Pakistan*; Graphic Publishers: Santa Ana, CA, USA, 1997.
30. Kadri, I.B. *Petroleum Geology of Pakistan*; Pakistan Petroleum Limited: Karachi, Pakistan, 1995.
31. Baig, M.; Snee, L. Pre-Himalayan dynamothermal and plutonic activity preserved in the Himalayan collision zone, NW Pakistan: An thermochronologic evidence. *Proc. Geol. Soc. Am. Abstr. Programs* **1989**, *21*, A268.
32. Munir, H.; Baig, M.S.; Mirza, K. Upper Cretaceous of Hazara and Paleogene Biostratigraphy of Azad Kashmir, North-West Himalayas, Pakistan. *Geol. Bull. Punjab. Univ* **2006**, *40–41*, 69–87.
33. Dunham, R.J. *Classification of Carbonate Rocks According to Depositional Textures*; American Association of Petroleum Geosciences: Tulsa, OK, USA, 1962.
34. Sibley, D.F.; Gregg, J.M. Classification of dolomite rock textures. *J. Sediment. Res.* **1987**, *57*, 967–975.
35. Shah, S. Stratigraphy of Pakistan (memoirs of the geological survey of Pakistan). *Geol. Surv. Pak.* **2009**, *22*, 1–381.
36. Wadia, D.N. The geology of Poonch State (Kashmir) and adjacent portions of the Punjab. *Mem. Geol. Surv. India* **1928**, *51*, 185–370.
37. Flügel, E.; Munnecke, A. *Microfacies of Carbonate Rocks: Analysis, Interpretation and Application*; Springer: Berlin/Heidelberg, Germany, 2010; Volume 976.
38. Logan, B.W.; Rezak, R.; Ginsburg, R. Classification and environmental significance of algal stromatolites. *J. Geol.* **1964**, *72*, 68–83. [CrossRef]
39. Kalkowsky, E. Oolith und Stromatolith im norddeutschen Buntsandstein. *Z. Dtsch. Geol. Ges.* **1908**, *60*, 68–125.
40. Logan, B.W. *Pressure Responses (Deformation) in Carbonate Sediments and Rocks Analysis and Application, Canning Basin*; American Association of Petroleum Geosciences: Tulsa, OK, USA, 1984.
41. Gee, E.; Gee, D. Overview of the geology and structure of the Salt Range, with observations on related areas of northern Pakistan. *Geol. Soc. Am.* **1989**, *232*, 95–112.
42. Pogue, K.R.; Wardlaw, B.R.; Harris, A.G.; Hussain, A. Paleozoic and Mesozoic stratigraphy of the Peshawar basin, Pakistan: Correlations and implications. *Geol. Soc. Am. Bull.* **1992**, *104*, 915–927. [CrossRef]
43. Calkins, J.A.; Tw, O.; Skm, A. *Geology of the Southern Himalaya in Hazara, Pakistan and Adjacent Areas*; US Government Prointing State Office: Washington, DC, USA, 1975.

44. Qasim, M.; Khan, M.A.; Haneef, M. Stratigraphic characterization of the Early Cambrian Abbottabad Formation in the Sherwan area, Hazara region, N. Pakistan: Implications for Early Paleozoic stratigraphic correlation in NW Himalayas, Pakistan. *J. Himal. Earth Sci.* **2014**, *47*, 25–40.
45. Gregg, J.M.; Bish, D.L.; Kaczmarek, S.E.; Machel, H.G. Mineralogy, nucleation and growth of dolomite in the laboratory and sedimentary environment: A review. *Sedimentology* **2015**, *62*, 1749–1769. [CrossRef]
46. Manche, C.J.; Kaczmarek, S.E. A global study of dolomite stoichiometry and cation ordering through the Phanerozoic. *J. Sediment. Res.* **2021**, *91*, 520–546. [CrossRef]
47. Machel Hans, G. Concepts and models of dolomitization: A critical reappraisal. *Geol. Soc. Lond. Spec. Publ.* **2004**, *235*, 7–63. [CrossRef]
48. Latif, M. Lower Palaeozoic (? Cambrian) hyolithids from the Hazara Shale, Pakistan. *Nat. Phys. Sci.* **1972**, *240*, 92. [CrossRef]
49. Haldar, S.; Tišljar, J. Basic mineralogy. In *Introduction to Mineralogy and Petrology*; Elsevier: Oxford, UK, 2014; p. 338.
50. Rahim, H.-u.; Qamar, S.; Shah, M.M.; Corbella, M.; Martín-Martín, J.D.; Janjuhah, H.T.; Navarro-Ciurana, D.; Lianou, V.; Kontakiotis, G. Processes Associated with Multiphase Dolomitization and Other Related Diagenetic Events in the Jurassic Samana Suk Formation, Himalayan Foreland Basin, NW Pakistan. *Minerals* **2022**, *12*, 1320. [CrossRef]
51. Ahmad, I.; Shah, M.M.; Janjuhah, H.T.; Trave, A.; Antonarakou, A.; Kontakiotis, G. Multiphase Diagenetic Processes and Their Impact on Reservoir Character of the Late Triassic (Rhaetian) Kingriali Formation, Upper Indus Basin, Pakistan. *Minerals* **2022**, *12*, 1049. [CrossRef]
52. Fang, Y.; Xu, H. Dissolved silica-catalyzed disordered dolomite precipitation. *Am. Mineral.* **2022**, *107*, 443–452. [CrossRef]
53. Fang, Y.; Xu, H. Coupled dolomite and silica precipitation from continental weathering during deglaciation of the Marinoan Snowball Earth. *Precambrian Res.* **2022**, *380*, 106824. [CrossRef]
54. Yang, X.; Tang, H.; Wang, X.; Wang, Y.; Yang, Y. Dolomitization by penesaline sea water in Early Cambrian Longwangmiao Formation, central Sichuan Basin, China. *J. Earth Sci.* **2017**, *28*, 305–314. [CrossRef]
55. Qing, H.; Bosence, D.W.J.; Rose, E.P.F. Dolomitization by penesaline sea water in Early Jurassic peritidal platform carbonates, Gibraltar, western Mediterranean. *Sedimentology* **2001**, *48*, 153–163. [CrossRef]
56. Yang, W.; Lehrmann, D.J. Milankovitch climatic signals in lower Triassic (Olenekian) peritidal carbonate successions, Nanpanjiang Basin, South China. *Palaeogeogr. Palaeoclimatol. Palaeoecol.* **2003**, *201*, 283–306. [CrossRef]
57. Banerjee, S.; Khanolkar, S.; Saraswati, P.K. Facies and depositional settings of the Middle Eocene-Oligocene carbonates in Kutch. *Geodin. Acta* **2018**, *30*, 119–136. [CrossRef]
58. Gao, X.; Wang, P.; Li, D.; Peng, Q.; Wang, C.; Ma, H. Petrologic characteristics and genesis of dolostone from the Campanian of the SK-I Well Core in the Songliao Basin, China. *Geosci. Front.* **2012**, *3*, 669–680. [CrossRef]
59. Budd, D.A.; Hiatt, E.E. Mineralogical stabilization of high-magnesium calcite; geochemical evidence for intracrystal recrystallization within Holocene porcellaneous foraminifera. *J. Sediment. Res.* **1993**, *63*, 261–274.
60. James, N.; Choquette, P. Diagenesis 9. Limestones-the meteoric diagenetic environment. *Geosci. Can.* **1984**, *11*, 161–194.
61. Palmer, A.N. Origin and morphology of limestone caves. *Geol. Soc. Am. Bull.* **1991**, *103*, 1–21. [CrossRef]
62. Smith, M.; Soper, N.; Higgins, A.; Rasmussen, J.; Craig, L. Palaeokarst systems in the Neoproterozoic of eastern North Greenland in relation to extensional tectonics on the Laurentian margin. *J. Geol. Soc.* **1999**, *156*, 113–124. [CrossRef]
63. Compton, J.S. Porosity reduction and burial history of siliceous rocks from the Monterey and Sisquoc Formations, Point Pedernales area, California. *Geol. Soc. Am. Bull.* **1991**, *103*, 625–636. [CrossRef]
64. Hesse, R. Silica diagenesis: Origin of inorganic and replacement cherts. *Earth-Sci. Rev.* **1989**, *26*, 253–284. [CrossRef]
65. Berra, F.; Angiolini, L. The Evolution of the Tethys Region throughout the Phanerozoic: A Brief Tectonic Reconstruction. *Pet. Syst. Tethyan Reg.* **2014**, *106*, 1–7. [CrossRef]
66. Kaczmarek, S.E.; Sibley, D.F. On the evolution of dolomite stoichiometry and cation order during high-temperature synthesis experiments: An alternative model for the geochemical evolution of natural dolomites. *Sediment. Geol.* **2011**, *240*, 30–40. [CrossRef]
67. Manche, C.J.; Kaczmarek, S.E. Evaluating reflux dolomitization using a novel high-resolution record of dolomite stoichiometry: A case study from the Cretaceous of central Texas, USA. *Geology* **2019**, *47*, 586–590. [CrossRef]